

**SUPER-RESOLUTION FOR ENHANCED AREA ESTIMATION
AND TARGET DETECTION**

A DISSERTATION

SUBMITTED IN PARTIAL FULFILMENT OF THE REQUIREMENTS
FOR THE AWARD OF THE DEGREE
OF

MASTER OF TECHNOLOGY
IN

CIVIL ENGINEERING

(With Specialization in Geoinformatics Engineering)

Submitted By:

UTKARSH KARN
(2K20/GEO/09)

Under the supervision of

DR. K.C. TIWARI, PROFESSOR



MULTIDISCIPLINARY CENTRE FOR GEOINFORMATICS

DEPARTMENT OF CIVIL ENGINEERING

DELHI TECHNOLOGICAL UNIVERSITY

(Formerly Delhi College of Engineering)

Bawana Road, Delhi – 110042

MAY 2022

DELHI TECHNOLOGICAL UNIVERSITY
(Formerly Delhi College of Engineering)
Bawana Road, Delhi – 110042

CANDIDATE’S DECLARATION

I, Utkarsh Karn, Roll No. 2K20/GEO/09 of M. Tech Geoinformatics Engineering, hereby declare that the project Dissertation titled “**Super-resolution for enhanced area estimation and target detection**” which is submitted by me to the Department of Civil Engineering, Delhi Technological University, Delhi in partial fulfilment of the requirement for the award of the degree of Master of Technology, is original and not copied from any source without proper citation. This work has not previously formed the basis for the award of any Degree, Diploma Associateship, Fellowship or other similar title recognition.

Place: Delhi

UTKARSH KARN

Date:

CIVIL ENGINEERING DEPARTMENT
DELHI TECHNOLOGICAL UNIVERSITY
(Formerly Delhi College of Engineering)
Bawana Road, Delhi – 110042

CERTIFICATE

I hereby certify that the Project Dissertation titled “**Super-resolution for enhanced area estimation and target detection**” which is submitted by Utkarsh Karn, Roll no. 2K20/GEO/09 [Civil Engineering], Delhi Technological University, Delhi in partial fulfilment of the requirement for the award of the degree of Master of Technology, is a record of the project work carried out by the students under my supervision. To the best of my knowledge this work has not been submitted in part or full for any Degree or Diploma to this University or elsewhere.

Place: Delhi

Date:

DR. K. C. TIWARI

SUPERVISOR

Professor, Civil Engineering
Delhi Technological University
(Formerly Delhi College of Engineering)
Bawana Road, Delhi – 110042

ABSTRACT

Low-resolution of satellite images restrict the performance and applications of satellite image processing. Due to inability of the methods to convert low-resolution satellite imagery to high-resolution, there might be a large amount of temporal data loss. Satellite imagery deals with the problem of mixed pixels and aims to minimise it. This study focuses on the review of the methods to classify subpixels inside the mixed pixels, along with the background involving endmember extraction and abundance mapping.

Further, the study utilises two subpixel mapping algorithms, i.e. Pixel Swap (PS) Method and Inverse Euclidean Distance (IED) Method for the subpixel distribution of binary classes. The model is trained on resampled satellite image to compute the best possible method among these to perform binary target detection. Considering various accuracy metrics, IED performs better than PS. This IED algorithm is further used on Landsat-8 data, with a scale factor 3, to obtain the high-resolution image. This high-resolution output image is used in the application of area estimation. In area estimation, the area corresponding to pure target pixels only is calculated for the reference image, the output image and the low-resolution image.

Accuracy of IED for testing was not as high as training. But, considering the increase in area estimation of the target from original low-resolution imagery to output high-resolution imagery, the method is reliable enough for subpixel mapping.

ACKNOWLEDGMENTS

First and foremost, I thank *the Almighty God*, for his strength, sustenance, and graces from the beginning of my academics up to this phase of being able to write the thesis for my master's degree.

My humble appreciation and gratitude are reserved and due for my impeccable and ever-supportive supervisor *Dr. K. C. Tiwari* for his quintessential guidance and empathetic approach towards me over all these years of doing research. The cooperation, appreciations, critics, and motivations received from him over this period helped in gracefully overcoming all the challenges and obstacles that came in the way.

I am indebted to the persistent support received from all the members of *The Multidisciplinary Centre for Geoinformatics*, Delhi Technological University, who have always been available at the need of the hour. I would like to recognize the invaluable assistance obtained from my *fellow batchmates* over all these months.

My words of thanks are due to all my near and dear ones including my family, relatives, and friends, for their mental support and understanding approach that kept me motivated.

Thank you so much everyone for standing beside me on this journey and keeping me work towards success.

UTKARSH KARN

CONTENTS

CANDIDATE’S DECLARATION	i
CERTIFICATE	ii
ABSTRACT	iii
ACKNOWLEDGMENTS	iv
CONTENTS	v
LIST OF FIGURES	vii
LIST OF TABLES	ix
CHAPTER 1: INTRODUCTION	1
1.1 General	1
1.2 Issues of Multi-Sensor Multi-Resolution Remote Sensing	2
1.3 Gaps In The Study	4
1.4 Motivation	4
1.5 Objectives	4
1.5 Organisation of Thesis	5
CHAPTER 2: CRITICAL REVIEW	6
2.1 Mixed Pixels and Spectral Unmixing	6
2.1.1. Endmember extraction	8
2.1.2. Spectral Unmixing and Fractional Abundance	11
2.2 Subpixel Mapping and Super Resolution	13
CHAPTER 3: IDENTIFICATION OF MODEL FOR SUPER RESOLUTION	17
3.1 Background	17

3.2	Datasets & Software Requirements	18
3.2.1	Datasets	18
3.2.2	Softwares	19
3.3	Methodology	19
3.3.1	Pixel Swap Algorithm	24
3.3.2	Inverse Euclidean Distance (IED) Algorithm	25
3.4	Results	27
3.4.1	Mean Square Error (MSE)	28
3.4.2	Structural Similarity Index (SSI)	28
3.4.3	Peak Signal to Noise Ratio (PSNR)	28
3.4.4	Model Conclusion	29
	CHAPTER 4: IMPLEMENTATION AND APPLICATIONS OF IED	30
4.1	Data and Methodology	30
4.1.1	Data Used	30
4.1.2	Methodology	30
4.2	Implementation	31
4.3	Area Estimation	36
4.4	Results and Discussion	37
4.4.1	Results	37
4.4.2	Discussion	37
	CHAPTER 5: CONCLUSION	38
	REFERENCES	39
	APPENDIX 1: Resampling Code	45
	APPENDIX 2: Preprocessing Of Data (MATLAB)	46
	APPENDIX 3: IED Technique (MATLAB)	47

LIST OF FIGURES

Figure 1.1	Pure and Mixed Pixels	2
Figure 2.1	Mixed Pixel Target	7
Figure 2.2	Fractional Abundance Maps	11
Figure 3.1	Binary image showing white target	17
Figure 3.2	Sentinel 2 Data in JPEG format (left) and TIFF format (right)	18
Figure 3.3	Linear Spectral Unmixing - Target (top) , Background (bottom left)	20
Figure 3.4	Abundance fraction of target endmember	21
Figure 3.5	Target image	21
Figure 3.6	Histogram of Original Image used to decide the threshold of the target	22
Figure 3.7	Methodology Flowchart	23
Figure 3.8	Output image by Pixel Swap	27
Figure 3.9	Output image by IED	27
Figure 4.1	Landsat 30 m Imagery	30
Figure 4.2	Flowchart of the methodology of testing	31
Figure 4.3	Endmember Selection using ROI tool in ENVI	32
Figure 4.4	Abundance Map of Target	32
Figure 4.5	Histogram of the Landsat Data	33
Figure 4.6	Target Image	34
Figure 4.7	Output after IED Algorithm	34

Figure 4.8	RGB Composite of Sentinel-2 data	35
Figure 4.9	Abundance map of Target (left) and Background (right)	35
Figure 4.10	Binary Image of Sentinel-2 for validation	36

LIST OF TABLES

Table 1.1 High-resolution Satellites and the cost of their imagery	3
Table 2.1 Review of Endmember Extraction Techniques	9
Table 2.2 Some Existing Super Resolution Techniques	15
Table 3.1 Sentinel 2 Data	19

LIST OF ABBREVIATIONS

AAAS	American Association for the Advancement of Science
AMEE	Automated Morphological Endmember Extraction
ANN	Artificial Neural Network
AVIRIS	Airborne Visible-Infrared Imaging Spectrometer
BFM	Bilinear-Fan Model
CCA	Convex Cone Analysis
CF	Correct Fraction
CRS	Coordinate Reference System
DEM	Digital Elevation Model
FCLS	Fully Constrained Least Squares
GA	Genetic Algorithm
GRP	Ground Reference Points
HNN	Hopfield Neural Network
IEA	Iterative Error Analysis
IED	Inverse Euclidean Distance
JPEG	Joint Photographic Experts Group
LIDAR	Light Detection and Ranging
LLM	Linear Mixture Model
LSU	Linear Spectral Unmixing

MEST	Manual Endmember Selection Tool
MRF	Markov Random Field
ORASIS	Optical Real-time Adaptive Spectral Identification System
POCS	Projection Onto Convex Sets
PPI	Pixel Purity Index
PPNM	Polynomial Post-Nonlinear Model
PS	Pixel Swap
PSNR	Peak Signal to Noise Ratio
PSO	Particle Swarm Optimisation
RFSR	Random Forest Super Resolution
RGB	Red Green Blue
RMSE	Root Mean Square Error
SAM	Sub-pixel/Pixel Attraction Model
SFCM	Supervised Fuzzy c-means
SMA	Spectral Mixture Analysis
SNR	Signal to Noise Ratio
SR	Super Resolution
SVM	Support Vector Machine
TIFF	Tag Image File Format
VDSR	Very Deep Super Resolution

CHAPTER 1

INTRODUCTION

1.1 GENERAL

Super-resolution is a type of image restoration that aims to turn low-quality images into high-resolution images [1]. It is similar to sub-pixel mapping, which is a technique for locating soft values inside each pixel and transferring fraction images to subpixel land cover maps using information supplied by soft categorization [2].

The method of acquiring data by measuring an area on the ground and assigning a value to it is known as remote sensing. Satellite remote sensing, being one of the methods for remote sensing, is improving all the time. The output of satellite remote sensing is present in the form of images, dealing with various types of resolutions, such as spatial resolution, spectral resolution, temporal resolution, and radiometric resolution.

Hyperspectral sensors give much more information per recorded pixel than multispectral sensors in the form of a three-dimensional cube comprising two spatial dimensions and one spectral dimension [3]. As a result, thorough examinations of the earth's characteristics are now feasible, which would otherwise be lost in low spectral resolution data [4] [5].

As there is an increase in spectral resolution of hyperspectral images, the spatial resolution usually gets worse [6]. For sensors at high altitudes which cover wide areas, low-resolution images are quite common as the introduction of high-resolution sensors on such platforms might increase the cost. The low resolution of hyperspectral images restricts the performance of algorithms for processing and analysing. In the process of classification, mixed pixels are created due to low resolution. Pixels that contain more than one land cover type are called mixed pixels [7]. Fig. 1.1 [3] shows the problem of mixed pixels.

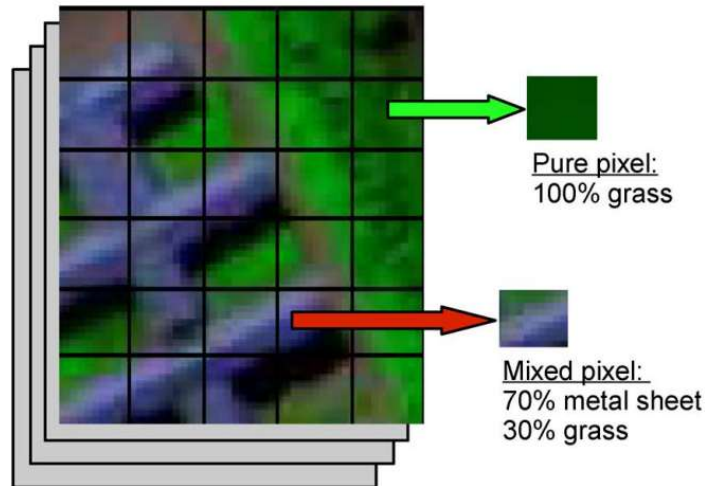


Figure 1.1 Pure and Mixed Pixels

Mixed pixels can be a difficult challenge because of the limited spatial resolution [8]. It leads to a reduction in accuracy and the performance of image analysis for detecting targets [9]. Several full-pixel techniques have been proposed during the last decade, however, these techniques are not suitable for mixed pixels due to high rates of error. To conduct mixed pixel analysis, it is necessary to separate the target from unwanted background information, which involves careful handling, investigation, and exploration [10]. Soft classification techniques are essentially used for this purpose [11].

Land cover classification, target detection, change detection, monitoring of vegetation, etc. describe some highlighting applications of hyperspectral images ([12] [13] [14]). Existing works for hyperspectral detection focus on the pixel level relying on spectral information and simple neighboring pixel correlation information [15]. The detection process can further be enhanced by exploiting the spatial correlation.

1.2 ISSUES OF MULTI-SENSOR MULTI-RESOLUTION REMOTE SENSING

For many years, high-resolution imagery has been obtained from space, mostly for military requirements [16] [17]. There are many satellite systems in orbit or scheduled that can give high-resolution images, such as the fine resolution sensing system from 0.6 m resolution of Quick Bird allows mapping at scales $\sim 1:5,000$ [18]. However, the main drawback of using these systems is the cost of imagery. Table 1.1 lists various satellite systems, along with their resolution and the cost of obtaining the data (according to the

American Association for the Advancement of Science (AAAS)). The cost of obtaining high-resolution imagery is extremely expensive for most of the applications. There are various satellite imagery portals such as Geocento and Apollo Mapping, which provide high-resolution imagery from various satellites by charging a large amount of money [19] [20]. Imagery from slightly coarser resolution systems such as SPOT costs about \$ 3-5 / km² and the extent covers a larger area [17]. Despite being costly, high-resolution images cover a smaller area on the ground. To cover an area the size of Oklahoma, US, at least four photos from the Pleiades-1, Kompsat-3, or SuperView-1 satellites would be required. A single Landsat 8 image, on the other hand, may cover the area of 25 such cities [21].

Low as well as medium-resolution imagery, however, provides less costly or free-of-charge images. The historical significance of such images is also relevant for various applications. However, the low level of detail is the main drawback [21].

Table 1.1 High-resolution Satellites and the cost of their imagery

Satellite	Resolution (in meters)	Price (Archived images)	Price (New Collection)
QuickBird	0.61 pan, 2.4 multi	\$ 17 / km ²	\$ 23 / km ²
Superview - 1	0.5 pan, 2 multi	\$ 14/ km ²	-
Worldview - 4	0.31 pan, 1.24 multi	\$ 22.5 / km ²	-
Worldview - 2	0.46 pan, 1.84 multi	\$ 17/ km ²	\$ 23 / km ²
Worldview – 1	0.4 pan	\$ 14 / km ²	\$ 20 / km ²
GeoEye – 1	0.41 pan, 1.65 multi	\$ 12.5 / km ²	\$ 25 / km ²
IKONOS	0.82 pan, 4 multi	\$ 10/ km ²	\$ 20 / km ²
PLEIADES NEO	0.3 pan, 1.2 multi	\$ 22.5/km ²	-
Kompsat-3	0.4 pan, 1.6 multi	\$ 12 / km ²	\$ 24 / km ²
SPOT- 6	2.2 pan, 8.8 multi	\$ 4.75 / km ²	-
Planetscope SI	3 pan	\$ 1.8 / km ²	-

1.3 GAPS IN THE STUDY

The research gaps observed in this study are

- i. There are various methods and techniques for endmember extraction and subpixel mapping. Selection of proper technique is essential. Hence, application-specific super resolution technique is needed to be adapted
- ii. Most of the subpixel mapping methods of super resolution consider the assumption of distribution of endmembers inside subpixel only on the basis of its abundance fraction.
- iii. The application of subpixel mapping in target detection and corresponding area estimation is very limited.

1.4 MOTIVATION

The motivation of this research comes from attending to the problem arising due to the low resolution of imagery obtained by the process of remote sensing. A few of the common problems, which require the need of super-resolution, are-

- i. Loss of temporal information: The data obtained during earlier times have low resolution. The inability of techniques to obtain information from this low-resolution data might result in huge temporal data loss for generations to come.
- ii. Inaccessible data capture: Data captured through various air platforms in enemy regions or regions, which cannot be accessed frequently, might come in low resolution.
- iii. Mixed pixels: Mixed pixels are a huge problem in hyperspectral imagery which further compromises with the process of target detection, land cover classification, change detection, etc.
- iv. High cost: Acquisition of high-resolution data requires the expenditure of a huge amount of money

1.5 OBJECTIVES

The objectives of this study are as follows

- i. Critical Review of the endmember extraction techniques and subpixel mapping techniques leading to super resolution
- ii. Development of a model for the super resolution to improve target detection
- iii. The utilisation of the model for enhanced area estimation

1.5 ORGANISATION OF THESIS

The work in this thesis is organised into five chapters, which include this introduction section.

Chapter-1 is dedicated to the overview of the topics to be addressed in the thesis, and the gaps identified that led to the motivation behind this research. The chapter is concluded with the definition of the objectives of the study.

Chapter 2 performs a critical review of endmember extraction techniques, spectral unmixing techniques, subpixel mapping techniques, and super resolution algorithms.

Chapter 3 covers the background, datasets, and methodology followed for implementing the algorithms. This chapter also covers and results and accuracy assessment of the model.

Chapter 4 describes the implementation and performance of the developed model. This chapter also deals with the application of area estimation using the model.

Chapter 5 Conclusion and future aspects

CHAPTER 2

CRITICAL REVIEW

2.1 MIXED PIXELS AND SPECTRAL UNMIXING

During the past decades, satellite photography has been subjected to a wide range of analytic approaches. They are either full pixel or mixed pixel approaches, in which each pixel vector in a hyperspectral picture encodes spectral information. Each pixel vector records the reaction of one mainly underlying substance at each point in a picture, which is the basic premise guiding full pixel approaches [22]. Mixed pixel approaches, on the other hand, are based on the notion that each pixel vector records the reaction of numerous underlying materials at each site. A scenario may emerge when neighbouring end members share a single pixel, resulting in the creation of mixed pixels [23]. Unfortunately, many sites in a picture are pure materials, but many others are mixes of elements, resulting in an image that is often a blend of the two conditions.

The approach of spectral matching is the most basic full-pixel methodology for satellite image analysis, mainly developed for hyperspectral imagery [24]. Spatial neighbours have no effect on the class label assignments supplied by spectral matching methods [23]. One of the most significant distinctions between pure and mixed pixel classification is that the former is a process of class membership assignment, whilst the latter is a method of endmember signature abundance estimate [25].

Jones and Sirault studied the effect of mixed pixels on thermal data too. They found the effects of increases in spatial resolution on the use of thermal imaging in-field plant phenotyping. When image pixels are significantly smaller than the objects of interest (e.g., leaves), accurate estimates of leaf temperature can be made; however, when pixels are on the same scale or larger than the objects of interest, the observed temperatures become significantly influenced by the background temperature due to the presence of mixed pixels. Approaches to estimating the true leaf temperature that work at both the whole-pixel and sub-pixel levels were examined and addressed [26].

Target identification using hyperspectral or multispectral images is important, especially for military applications. Spectral variation and subpixel target detection are the two most challenging aspects of target detection. Because of the spatial resolution limits, the ground sample distance is frequently longer than the size of the targets of interest, resulting in mixed pixels. This, in turn, makes it difficult to determine the target pixel through its spectra, especially if the target is very small. Figure 2.1 shows the subpixel target in a mixed pixel.

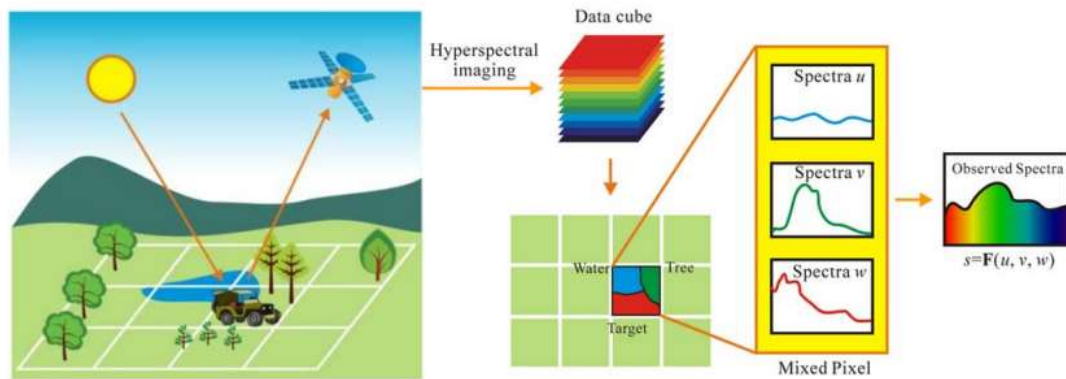


Figure 2.1 Mixed Pixel Target [27]

By combining linear statistical modeling and signal processing techniques, spectral mixture analysis (SMA) techniques have solved some of the shortcomings of full pixel approaches [28] [29]. They are either nonlinear or linear approaches by definition. Nonlinear mixed pixel analysis necessitates a thorough understanding of numerous scattering effects that may develop as a result of the close proximity of components inside each pixel [30]. Although sub-pixel nonlinear mixing is useful for some types of analysis, the effects of multiple scattering are thought to be minimal in the majority of cases if a linear model is utilised [31].

Spectral Mixture Analysis accepts the fact that the spectrum which is measured for a mixed pixel is a function of the pure spectral features, called endmembers, present in that pixel, with their corresponding weighting factors. This Spectral Mixture Analysis is also called Spectral Unmixing. For target detection algorithms, spectral unmixing is performed to separate the target spectra from the background spectra [32]. Spectral unmixing provides the end member present within the pixel and their corresponding abundance fractions (discussed in the next subsection). Spectral unmixing involves two

processes, namely, endmember extraction and creation of abundance map using abundance fraction.

2.1.1. Endmember extraction

An endmember is a surface material's spectrally distinct, idealised, and pure signature [33]. Endmembers can be gathered in one of two ways: either by ground truthing to produce ground reference points (GRPs) or through image data extraction to obtain GRP surrogates, or both [34]. Collecting a significant number of high-quality field samples is frequently a costly and time-consuming undertaking, especially in places with difficult terrain or inaccessibility. Algorithms are used to obtain training samples from remotely sensed images themselves. Thus, generating pure full pixel endmembers from an image is termed as 'Endmember Extraction' [3] [8].

A study by Pablo J. Martinez et.al [35], summarised that the best endmembers must be obtained in the same condition as the unmixing spectrum (from the same image) preventing external factors, such as the illumination or elevation angles, affecting the unmixing results. The endmember extraction methods that jointly exploit spatial and spectral information obtain better quality endmembers than those methods which only utilize spectral information.

Table 2.1 summarises common endmember extraction methods. A study by Rui Song et.al [36], found that N-FINDR, which is one of the earliest endmember extraction algorithms, is employed in the framework to extract pure endmember pixels from Sentinel-2 spectral surface reflectance. Based on the pure spectra that are extracted from N-FINDR, a Fully Constrained Least Squares (FCLS) is employed to estimate the abundance map for each single pure spectrum

According to Plaza et.al [37], for mixed pixels containing binary components (synthetic data), PPI, N-Findr, CCA, and ORASIS are more sensitive to noise than IEA and AMEE. IEA and AMEE however produce the best similarity score for reflectance as well as radiance data. It has also been observed that the shade component is difficult to model. For abundance estimation, AMEE and IEA produce the lowest error score for high SNR. Performance increases with high SNR (for binary mixture). For non-binary mixture (synthetic data), AMEE scores are better. For real hyperspectral images, reflectance data

is better. For radiance data, AMEE is best. For reflectance, AMEE is best. Shade constituent is characterized better in IEA.

Table 2.1 Review of Endmember Extraction Techniques

Name of Method	Type	Ground Truth	Number of endmembers	Information used	Limitation
Manual Endmember Selection Tool (MEST) [38]	Supervised	Preferred, but not necessary	Pre-defined	Spectral information	Requires human intervention
Pixel Purity Index (PPI) [39] [40]	Supervised	Not used	Pre-defined is preferable	Spectral information	Sensitive to number of skewers and interactive tool is required for final endmember selection
N- FINDR [41] [42]	Automated	Reference spectra and abundance fraction	Random endmember for initialisation	Spectral information	Computational complexity and use of random initial endmembers
Iterative Error Analysis (IEA) [43] [44]	Automated	Reference spectra	Random initialisation vector, then provided	Spectral information	Discrimination between similar spectral vector is difficult because it ignores positive and

Table 2.1 (continued)

Name of Method	Type	Ground Truth	Number of endmembers	Information used	Limitation
Convex Cone Analysis (CCA) [45]	Automated	Reference spectra and abundance fraction	Endmembers form corners of convex cone	Spectral Information	High complexity for large number of endmembers
Automated Morphological Endmember Extraction (AMEE) [46]	Automated	Reference spectra and abundance fraction	Determined	Spectral and Spatial Information	Degree of purity of a pixel is not defined
Optical Real-time Adaptive Spectral Identification System (ORASIS) [47]	Automated	None	All standard spectra found in the imagery	Spectral information	Simple shrinking algorithm

2.1.2. Spectral Unmixing and Fractional Abundance

The goal of spectral unmixing is to determine the fractional abundance of the various components that appear inside the mixed pixels [38]. Spectral unmixing produce a habitat map for classes, that is fundamentally different from a traditional per-pixel categorization. The fraction of an end member inside a mixed pixel is known as the fractional abundance of that end member. Figure 2.2 shows the fractional abundance map of three endmembers namely Endmember 1, Endmember 2, Endmember 3, and Endmember 4, where dark red shows the highest fraction of that endmember in the corresponding area.

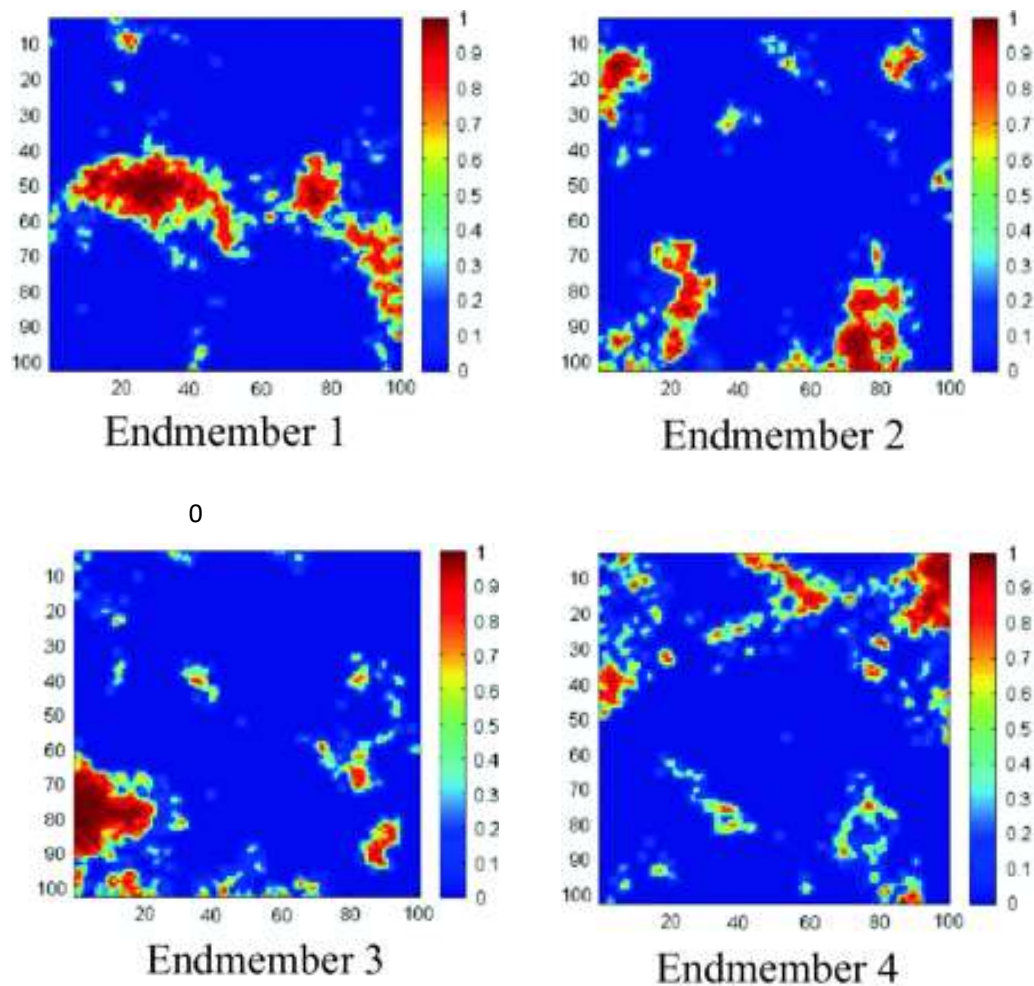


Figure 2.2 Fractional Abundance Maps [39]

The standard technique of spectral unmixing involves the linear combination of end-members, weighted by their respective abundance fractions. This technique is called Linear Mixture Model (LMM). In most cases, the LMM is simple to use and adaptable. The model is described by

$$s_n(\lambda) = \sum_{k=1}^p f_k es_k(\lambda) \quad (2.1)$$

$$\sum_{k=1}^p f_k = 1.0 \quad 0 \leq f_k < 1.0 \quad (2.2)$$

where $s_n(\lambda)$ is the surface reflectance curve of a mixed sample, $es_k(\lambda)$ is the surface reflectance curve of the k th endmember, f_k is the abundance of k th endmembers in a mixed sample, and p are the endmembers that exist in the data [38]. A study conducted by Zhang, Rivard, and Sanchez-Azofeifa found that if the endmembers in mixed samples are linearly mixed, the derivative will follow the linearity as well [40]. The capacity to resolve absorption characteristics and define their typical forms and precise wavelength area is a benefit of the spectral derivative [40]. Since it typically consists of an appropriate first-order approximation of the physical processes involved in most scenes of interest, the LMM has gotten a lot of attention [41].

In the study conducted by Yu, Chen, Lin, and Ye [42], multispectral data is used to compare the performance of six linear and nonlinear unmixing approaches: supervised fuzzy c-means (SFCM), fully constrained least squares (FCLS), artificial neural network (ANN), polynomial post-nonlinear model (PPNM), bilinear-Fan model (BFM), and Support Vector Machine (SVM). By evaluating the indicators of accuracy such as, RMSE and Pearson correlation coefficient (r). The results of the unmixing were evaluated in terms of overall performance, pure and mixed data sets, and sub-scenes with different mixture proportions.. In various research regions, the performance of nonlinear techniques varied drastically as the number of mixed pixels rose. When the fraction of mixed pixels was high, SVM, SFCM, BFM, and PPNM performed better, however, ANN performed better when processing vast numbers of relatively clean pixels. The proportion change of mixed pixels in a research region affects the performance of nonlinear techniques considerably. The linear technique, on the other hand, is better for an

approximate estimate, especially if you have limited prior information on the subject topic.

Although the physical relevance of LMM is assured by equation (2.1), precise abundance assessment would be extremely difficult. Unlike multispectral unmixing, which focuses on accurate measurement of a single signature, target detection focuses on its presence, which may be assessed by the relative value of abundance, with the bigger abundance indicating a target sample and the lesser abundance indicating a background sample [43].

2.2 SUBPIXEL MAPPING AND SUPER RESOLUTION

The practise of optimising abundance fractions within or between pixels in order to create a subpixel map with a spatial resolution finer than the coarse spatial resolution input picture is known as super resolution [44]. It combines sub-pixel information in images to boost the image's resolution. Estimation of class proportion inside a pixel is called subpixel mapping. This sort of land-cover mapping, which was first described by Atkinson [45], can be thought of as post-processing of soft categorization. As a result, super resolution mapping algorithms employ the fraction values obtained from soft categorization as input to find a suitable geographic position for specified land-cover fractions. Because there is no knowledge of subpixel proportion, super resolution mapping always creates ambiguity [46]. In order to reduce the uncertainty, more site-specific information at the sub-pixel scale would be beneficial. Panchromatic band images [47] [48], light detection and ranging (Lidar) data [48], digital elevation model (DEM) data [48], and vector boundaries [49], all contain this type of additional information for super-resolution mapping issues [50].

Deshpande and Patavardhan [51] performed a review of techniques involving super resolution and came out with the following observations:

- i. High-frequency content lost during the image acquisition process has to be recovered in the SR techniques
- ii. Frequency domain-based super resolution includes Fourier transform-based and wavelet transform based techniques

- iii. Interpolation-based (non-adaptive and adaptive) super resolution, reconstruction-based (deterministic and stochastic), and learning-based approaches are all examples of spatial domain-based super resolution.
- iv. SR approaches based on interpolation work well in smooth areas but poorly in edge areas.
- v. In the first stage, researchers switched their focus away from frequency-domain algorithms and toward spatial domain algorithms. In the second stage, regularised multi-frame SR frameworks were the major emphasis. Because of their effectiveness, the GPR and TV frameworks have become the most often used methodologies.

Subpixel mapping techniques for super resolution can be classified into two types:

- i. *Regression-based*, which includes
 - a. Geostatistical methods
 - b. Spatial Attraction Models
 - c. Random Forest Super Resolution (RFSR)
 - d. Artificial Neural Network (ANN)
 - e. Wavelet Transform
 - f. Projection Onto Convex Sets (POCS)
- ii. *Spatial Optimisation based*, which includes
 - a. Genetic Algorithms
 - b. Pixel Swapping
 - c. Hopfield Neural Network (HNN)
 - d. Markov Random Field (MRF)
 - e. Particle Swarm Optimisation

Table 2.2 covers major super resolution techniques used for satellite remotely sensed images. Challenges when applying super resolution algorithms include:

- i. The dimensionality of multispectral and hyperspectral data is larger.
- ii. Atmospheric conditions, haze, clouds, and cloud shadows add additional variation to measured values.
- iii. Characteristics vary globally for classes in imagery.

Table 2.2 Some Existing Super Resolution Techniques

Name	Properties	Limitation
Very Deep Super-Resolution (VDSR) [52]	Ability to train for multiple levels of enhancement Fast inference speed	Low convergence rate
Random Forest Super Resolution (RFSR) [53]	Fast inference speed Clustering-based method	Different discriminative characteristics are required for clustering and regression issues.
Projection Onto Convex Sets (POCS) [54]	Utilises wavelet bi-cubic interpolation algorithm and bilateral filtering	Extremely sensitive to knowledge
Genetic Algorithm (GA) [55]	Operates on a set of solutions and spatial dependence	Optimisation of GA Algorithms
Sub-pixel/Pixel Attraction Model (SAM) [56]	Spatial Dependence and it can be sub-pixel/sub-pixel attraction, sub-pixel/pixel attraction and pixel/pixel attraction	Does not consider the correlation between sub-pixels

Table 2.2 (Continued)

Name	Properties	Limitation
ANN Predicted Wavelet Transform [57] [58]	Approximation fraction image and estimated detailed coefficients are used to create a high resolution source image	Forecasting the border between classes is only accurate for particular classes.
Hopfield Neural Network (HNN) [59]	Spatial distribution formulated as a constraint satisfaction problem	Produce rounded corners and require the definition of pure pixels
Markov Random Fields (MRF) [60] [61]	Allows modeling of image's global spatial context using local interactions between class labels in a neighbourhood	Require input parameters to get good quality images and neighbourhood size is fixed
Particle Swarm Optimisation (PSO) [62] [63]	Based on social intelligence and fitness score of particles (pixels)	Low convergence rate in the process of iteration
Pixel Swap [64] [65]	Method with CF constraint and maintains the composition of the class	Intensive computation for large scale factors and does not consider the correlation between subpixels
Inverse Euclidean Distance (IED) [66]	It uses abundance fraction and works on the binary class problem	Non-recursive algorithm and use of linear Euclidean Distance for measurement of attraction

CHAPTER 3

MODEL FOR SUPER RESOLUTION

3.1 BACKGROUND

This section of Chapter 3 highlights the background essential to performing the research work. The critical review of the literature leading to the process of super resolution provided the necessary insights to be undertaken for this research.

The study mainly deals with the application of super resolution for target detection. Hence, the source images are conformed as a binary image. Binary pictures contain just two potential intensity values for each pixel [67]. They're usually shown in black and white. Figure 3.1 shows a binary image corresponding to target detection, marked by the red square.

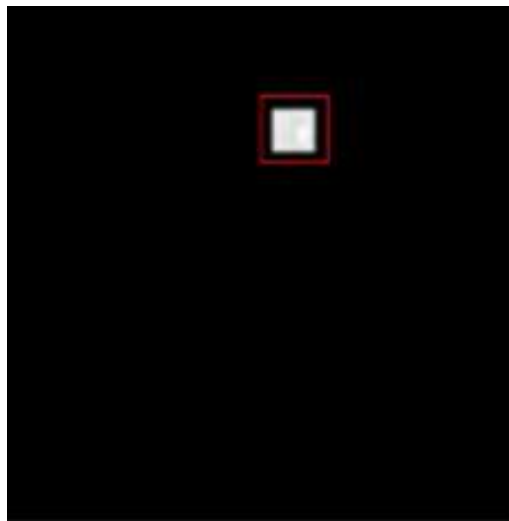


Figure 3.1 Binary image showing white target [68]

According to the previous chapter, the process of super resolution involves three basic steps. Endmember selection or extraction, abundance mapping, and subpixel mapping. Since the study is dealing with only the target and the rest of the classes in the image are considered as background, MEST is the adopted method for endmember selection. This method involves maximum human intervention and is supervised enough to be used for target detection. After the process of endmember selection, abundance maps involving the target and background as two defined classes (or endmember) are prepared

by the process of Linear Spectral Unmixing (LSU). LSU is used for the study due to its simplicity, ease to use, adaptability, and good approximation nature.

After LSU, the process of sub-pixel mapping is to be applied. Two techniques of subpixel mapping, namely, Pixel Swap (PS) and Inverse Euclidean Distance (IED) are being compared for the model. The technique with better results will be used for further applications. Pixel Swap, being one of the common and easy-to-use subpixel mapping algorithms, works on the random allocation of subpixels inside a pixel. This random distribution is based only on the fraction of each class/endmember inside the impure pixel. Most of the super resolution techniques are based on this random and recursive approach. However, IED is the non-random and non-recursive-based technique of subpixel mapping.

3.2 DATASETS & SOFTWARE REQUIREMENTS

3.2.1 Datasets

Data used in the model is from Sentinel-2 imagery collection. An image tile is downloaded from Google Earth Engine with minimal cloud cover and good visibility of the considered target object. Table 3.1 shows the specifications of the downloaded image. Figure 3.2 shows the image which is used to create input data, in jpeg format and tiff format (RGB).



Figure 3.2 Sentinel 2 Data in JPEG format (left) and TIFF format (right)

Table 3.1 Sentinel 2 Data

Type of Image	Residential
CRS	EPSG: 32631- WGS 84 / UTM Zone 31 N
Width	90
Height	90
Bands	13
Pixel size	10 × 10
Target	Central

3.2.2 Softwares

Various softwares necessary to perform the operations of the research are

- i. *Google Earth Engine*: To download data
- ii. *ArcMap 10.8*: For geospatial data handling
- iii. *ENVI Classic 5.3*: For satellite image processing
- iv. *Google Colab*: For the coding environment
- v. *MATLAB R2019a*: For model preparation and implementation

3.3 METHODOLOGY

The study aims to apply two super resolution techniques, i.e. pixel swap and inverse Euclidean distance on a Sentinel-2 image containing a target object. The A 90 × 90 image of pixel size 10 m is downloaded and resampled to 30 m pixel size using the bilinear technique, since visually most plausible downsample results are obtained using this technique [69]. After downsampling, the image is converted into a 30 × 30 image of pixel size 30 m. MEST is used on this 30 × 30 image in ENVI Classic 5.3 with two

endmembers, the target, and the background. LSU is then used to obtain the abundance map of the target, the background, and the error image (Figure 3.3).

The target abundance map showing the abundance fraction of the target in each pixel is imported in MATLAB R2019a for further processing. Figure 3.4 shows the normalised fractional abundance of the input data in the form of a 2D array in MATLAB.



Figure 3.3 Linear Spectral Unmixing - Target (top) , Background (bottom left) and Error (bottom right)

0.18	0.14	0.35	0.29	0.18	0.25	0.34	0.21	0.07	0.06	0.07	0.03	0.02	0.00	0.00	0.04	0.25	0.38	0.29	0.16	0.14	0.00	0.14	0.14	0.00	0.00	0.14	0.14	0.14	0.00
0.10	0.25	0.32	0.20	0.21	0.31	0.35	0.29	0.20	0.19	0.19	0.13	0.09	0.04	0.01	0.14	0.36	0.42	0.33	0.04	0.04	0.11	0.25	0.35	0.11	0.11	0.25	0.35	0.04	0.00
0.07	0.14	0.35	0.29	0.18	0.25	0.34	0.21	0.07	0.06	0.07	0.03	0.02	0.00	0.00	0.04	0.25	0.38	0.29	0.16	0.14	0.07	0.14	0.29	0.07	0.07	0.14	0.29	0.14	0.00
0.11	0.25	0.32	0.20	0.21	0.31	0.35	0.29	0.20	0.19	0.19	0.13	0.09	0.04	0.01	0.14	0.36	0.42	0.33	0.04	0.04	0.11	0.25	0.18	0.11	0.11	0.25	0.18	0.04	0.00
0.09	0.29	0.23	0.21	0.35	0.44	0.55	0.75	0.70	0.63	0.55	0.47	0.33	0.22	0.21	0.26	0.35	0.41	0.33	0.15	0.12	0.09	0.29	0.25	0.09	0.09	0.29	0.25	0.12	0.00
0.15	0.33	0.25	0.37	0.45	0.47	0.65	0.98	1.00	0.99	0.95	0.82	0.46	0.30	0.27	0.29	0.35	0.44	0.30	0.20	0.18	0.15	0.33	0.34	0.15	0.15	0.33	0.34	0.18	0.00
0.33	0.37	0.38	0.44	0.46	0.48	0.62	0.85	0.89	0.90	0.89	0.79	0.65	0.74	0.71	0.67	0.62	0.49	0.30	0.16	0.12	0.33	0.37	0.21	0.33	0.33	0.37	0.21	0.12	0.00
0.39	0.39	0.41	0.45	0.46	0.49	0.68	0.92	0.95	0.95	0.91	0.81	0.84	0.98	1.00	1.00	0.90	0.59	0.33	0.18	0.14	0.39	0.39	0.07	0.39	0.39	0.39	0.07	0.14	0.00
0.41	0.39	0.43	0.46	0.48	0.53	0.72	0.91	0.95	0.96	0.96	0.86	0.91	0.98	1.00	1.00	0.97	0.67	0.35	0.18	0.15	0.41	0.39	0.06	0.41	0.41	0.39	0.06	0.15	0.00
0.41	0.39	0.46	0.51	0.56	0.76	0.84	0.83	0.86	0.82	0.83	0.78	0.84	0.87	0.90	0.95	0.92	0.69	0.42	0.23	0.17	0.41	0.39	0.07	0.41	0.41	0.39	0.07	0.34	0.41
0.34	0.38	0.47	0.56	0.65	0.91	0.96	0.91	0.98	0.86	0.91	0.84	0.92	0.88	0.87	0.89	0.84	0.83	0.68	0.60	0.51	0.34	0.38	0.03	0.34	0.34	0.38	0.03	0.35	0.34
0.21	0.34	0.51	0.61	0.69	0.95	0.96	0.93	0.99	0.87	0.95	0.87	0.99	0.93	0.96	0.96	0.92	0.98	0.87	0.99	0.91	0.21	0.34	0.02	0.21	0.21	0.34	0.02	0.24	0.21
0.18	0.35	0.53	0.56	0.65	0.95	0.94	0.94	0.98	0.88	0.95	0.87	1.00	0.94	1.00	0.99	0.95	1.00	0.92	1.00	0.97	0.18	0.35	0.00	0.18	0.18	0.35	0.00	0.15	0.18
0.15	0.24	0.45	0.52	0.67	0.94	0.93	0.96	0.97	0.89	0.93	0.89	1.00	0.95	1.00	1.00	0.99	1.00	0.96	1.00	0.95	0.15	0.24	0.00	0.15	0.15	0.24	0.00	0.12	0.15
0.15	0.15	0.34	0.49	0.61	0.80	0.82	0.88	0.90	0.86	0.90	0.88	0.98	0.93	1.00	1.00	0.99	1.00	0.94	0.15	0.15	0.04	0.15	0.15	0.04	0.15	0.15	0.04	0.09	0.15
0.15	0.12	0.22	0.43	0.47	0.49	0.62	0.85	0.89	0.88	0.89	0.84	0.85	0.87	0.92	0.89	0.93	0.93	0.89	0.96	0.87	0.15	0.12	0.25	0.15	0.15	0.12	0.25	0.02	0.15
0.11	0.09	0.10	0.27	0.38	0.33	0.55	0.87	0.95	0.97	0.99	0.91	0.86	0.96	0.96	0.94	0.93	0.83	0.62	0.61	0.61	0.11	0.09	0.38	0.11	0.11	0.09	0.38	0.07	0.11
0.05	0.02	0.00	0.08	0.31	0.34	0.45	0.63	0.68	0.75	0.80	0.76	0.78	0.87	0.90	0.92	0.93	0.79	0.52	0.49	0.49	0.05	0.02	0.29	0.05	0.05	0.02	0.29	0.14	0.05
0.15	0.07	0.00	0.00	0.14	0.31	0.38	0.47	0.49	0.51	0.53	0.52	0.53	0.56	0.59	0.62	0.62	0.58	0.47	0.44	0.46	0.15	0.07	0.33	0.15	0.15	0.07	0.33	0.04	0.15
0.25	0.15	0.07	0.00	0.00	0.18	0.35	0.44	0.52	0.55	0.56	0.55	0.56	0.54	0.53	0.53	0.50	0.47	0.45	0.43	0.45	0.25	0.15	0.37	0.25	0.25	0.15	0.37	0.12	0.25
0.32	0.25	0.13	0.05	0.00	0.02	0.22	0.29	0.34	0.34	0.37	0.41	0.43	0.46	0.48	0.50	0.49	0.45	0.44	0.44	0.46	0.32	0.25	0.39	0.32	0.32	0.25	0.39	0.18	0.32
0.33	0.14	0.22	0.13	0.02	0.00	0.35	0.14	0.14	0.18	0.14	0.22	0.22	0.35	0.22	0.14	0.22	0.29	0.14	0.22	0.43	0.33	0.14	0.39	0.33	0.33	0.14	0.39	0.12	0.33
0.33	0.04	0.18	0.13	0.04	0.02	0.32	0.04	0.04	0.07	0.25	0.18	0.22	0.32	0.22	0.25	0.18	0.29	0.25	0.18	0.43	0.33	0.04	0.39	0.33	0.33	0.04	0.39	0.14	0.33
0.18	0.12	0.09	0.13	0.02	0.01	0.23	0.12	0.12	0.19	0.29	0.09	0.22	0.35	0.22	0.29	0.09	0.29	0.09	0.49	0.18	0.12	0.38	0.18	0.18	0.12	0.38	0.15	0.18	
0.09	0.18	0.21	0.13	0.01	0.02	0.25	0.18	0.18	0.07	0.33	0.21	0.22	0.32	0.22	0.33	0.21	0.29	0.33	0.21	0.38	0.09	0.18	0.34	0.09	0.09	0.18	0.34	0.17	0.09
0.21	0.12	0.22	0.13	0.02	0.04	0.38	0.12	0.12	0.38	0.37	0.22	0.22	0.23	0.22	0.37	0.22	0.29	0.37	0.22	0.34	0.21	0.12	0.35	0.21	0.21	0.12	0.35	0.33	0.21
0.22	0.14	0.25	0.23	0.13	0.11	0.41	0.14	0.14	0.15	0.39	0.25	0.23	0.25	0.18	0.39	0.25	0.21	0.39	0.25	0.34	0.22	0.14	0.24	0.22	0.22	0.14	0.24	0.39	0.22
0.29	0.15	0.25	0.23	0.13	0.11	0.19	0.15	0.15	0.15	0.22	0.25	0.23	0.38	0.18	0.21	0.25	0.21	0.17	0.25	0.18	0.29	0.15	0.15	0.29	0.29	0.15	0.15	0.41	0.29
0.31	0.17	0.22	0.23	0.13	0.11	0.13	0.17	0.17	0.10	0.22	0.22	0.23	0.22	0.18	0.21	0.22	0.21	0.17	0.22	0.38	0.31	0.17	0.12	0.31	0.31	0.17	0.12	0.41	0.31
0.29	0.24	0.25	0.23	0.13	0.11	0.19	0.11	0.11	0.15	0.22	0.25	0.23	0.14	0.18	0.21	0.25	0.21	0.17	0.25	0.34	0.29	0.24	0.09	0.29	0.29	0.24	0.09	0.34	0.29

Figure 3.4 Abundance fraction of target endmember

The target here corresponds to pixels having a normalised abundance fraction of more than 0.78. Therefore, assigning value 0 to pixels having normalised abundance fraction less than 0.78, and keeping the values of pixels having values more than 0.78. Padding is also done at the boundaries to move the target towards the center. Figure 3.5 shows the image which shows only pixels having values more than 0.78. The histogram of the original image helps in deciding the threshold of the pixel value to define the target (Figure 3.6).

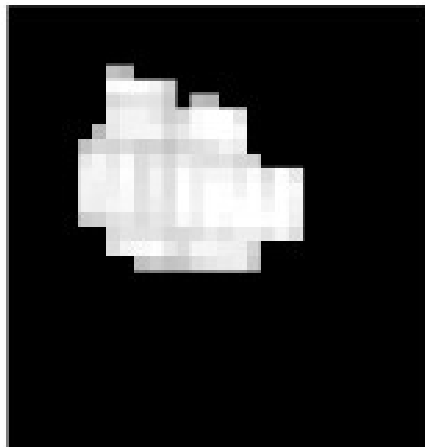


Figure 3.5 Target image

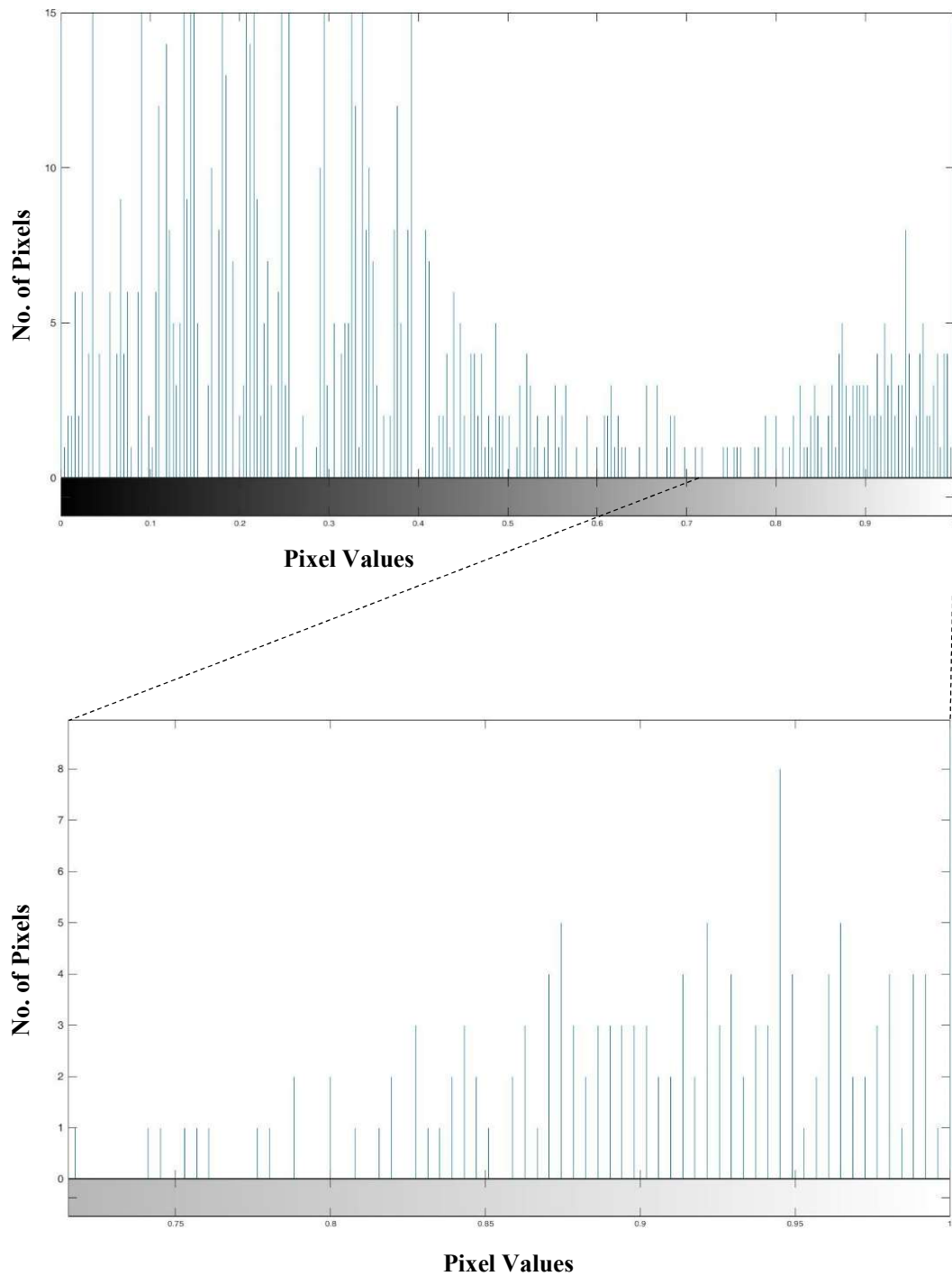


Figure 3.6 Histogram of Original Image used to decide the threshold of the target

The target image is provided for super resolution using Pixel Swap and Inverse Euclidean Distance algorithm with a scale factor of 3. Figure 3.7 shows the flowchart of the methodology followed.

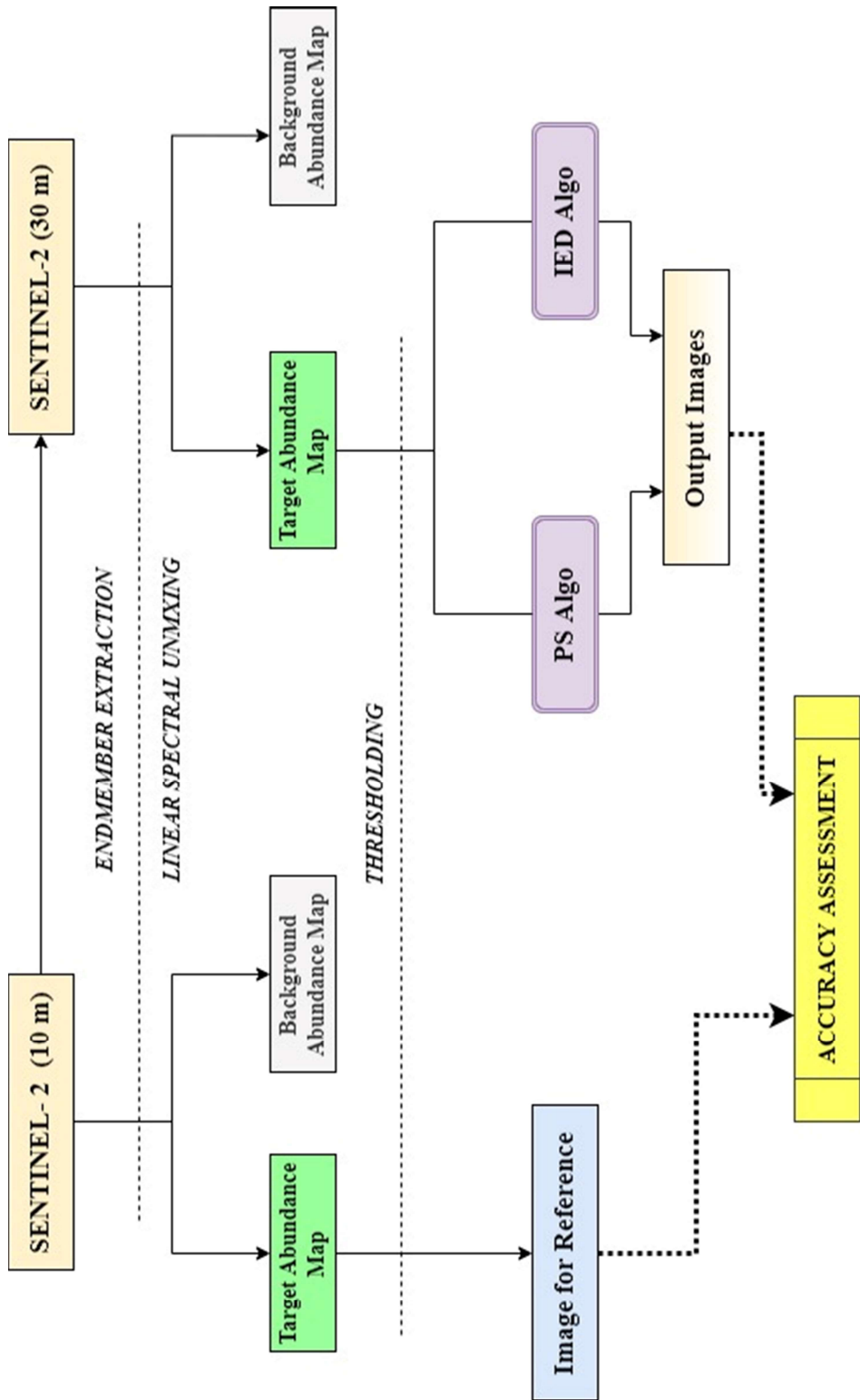


Figure 3.7 Methodology Flowchart

3.3.1 Pixel Swap Algorithm

The goal of this approach by Atkinson [64] [65] is to optimise the spatial correlation between nearby subpixels by changing the spatial layout of subpixels. The method considers a random initialization, and it also aims to determine the spatial arrangement of subpixels and works in a recursive way to determine their right allocation by determining the greatest correlation among surrounding subpixels. However, this approach only works for binary class problems, not multiclass problems.

Each pixel is split into a group of normally equal-sized sub-pixels when using the PS technique of super-resolution mapping. The scale factor is the percentage increase in spatial resolution from pixel to subpixel [70]. Abundance fractions of each class act as the input for the pixel swap algorithm. The quantity of subpixels that belongs to each pixel of images having low spatial resolution picture is determined using the scale factor.

The stages for putting the algorithm into action include random allocation of subpixels to binary classes based on the abundance proportion. For each subpixel within the pixel, attractiveness is calculated for each neighbouring subpixel within the kernel. The attractiveness is calculated as,

$$A_i = \sum_{j=1}^J \lambda_{ij} v(x_j) \quad (3.1)$$

A_i is the attractiveness of a subpixel i . $j = 1, 2, 3, \dots, J$ neighbouring subpixels. $v(x_j)$ is the binary class (1 or 0) of the j th subpixel at location x_j , and λ_{ij} is the weight function which is dependent on distance.

The attractiveness is predicted as a distance weighted function of its neighbours. If the minimum attractiveness of one pixel, is less than the maximum attractiveness of the second pixel, the single pair is swapped. This process is continued until no swaps can be made [65].

For large-scale factors, the swapping becomes intensive and the computation power increases. PS is particularly sensitive to the correctness of the soft

categorization since it slavishly retains the class composition information supplied by it [70].

3.3.2 Inverse Euclidean Distance (IED) Algorithm

The review of the study which introduced the concept of IED [66] [71] highlights the following points:

- i. Linear mixture model, constrained linear mixing model, MLP, and fuzzy methods involving neural networks can be used to recover components inside a pixel.
- ii. The proportional proportions of abundance fractions and their spatial distribution within pixels are not the same.
- iii. The first dataset is made up of synthetic data (subpixel abundance in known), whereas the second dataset is made up of AVIRIS data.
- iv. In Euclidean Distance based super resolution:
 - a. All subpixels exclusive to a pixel that belongs to a given class can be assumed to experience an attraction towards the centermost subpixel. This attraction is a function of the distance of any given subpixel from the centermost pixel.
 - b. Modeling attractive influence involves right distance function, quantity of subpixels belonging to each class, and a neighborhood scheme of pixels.
 - c. The scale factor corresponding to that pixel is used to calculate the number of subpixels in the coarse spatial resolution image. The scale factor is the number of rows and columns by which a pixel is split.
 - d. Pixel neighborhood signifies the collection of pixels that exert or experience attraction on/from the central pixel/subpixel. The pixel neighborhood scheme and object/class center concepts are used in the estimation of subpixel distances.

- e. A clique is a subset of an image array consisting of two different components that are common neighbours. They choose the number of pixels that have a direct impact on the pixel that is super resolved.
 - f. A pixel with a higher abundance percentage would pull in more subpixels from a super resolved pixel.
 - g. The attraction felt by each subpixel is inversely proportional to its distance from any of the adjoining pixels.
 - h. In using inverse Euclidean distance, the start location (the class/object center which is expected to exert attractive influence on the subpixels being super resolved) and finish location (the subpixel of the array on which the attractive influence is being estimated) are to be determined.
- v. This approach is based on the stored rankings of attractiveness values of the super-resolved subpixels and does not require iterative convergence.

Appendix 2 shows the MATLAB code that involves the implementation of this IED technique over the binary image. The steps involved in this process are:

- i. The judgment of the scale factor is done by trial and error.
- ii. The attractiveness of each pixel is defined as,

$$A_{ij} = \left(\frac{1}{d_{ij}} \right) \quad (3.2)$$

where d_{ij} is the Euclidean distance given by,

$$d_{ij} = \sqrt{(i - x_c)^2 + (j - y_c)^2} \quad (3.3)$$

where x_c and y_c are the coordinates of the subpixel facing the computed attractive impact, along with i and j are the coordinates of the neighbouring pixel's row as well as column presumed to be the start point.

- iii. Arrange A_{ij} in decreasing order and stored distinctly for each of the clique pixels.

- iv. The number of pixels corresponding to each clique pixels is calculated and super resolution is commenced.

3.4 RESULTS

The outputs of the algorithms is shown in Figure 3.8 and Figure 3.9. The output provided by the IED algorithm is much more accurate in terms of visual observation.

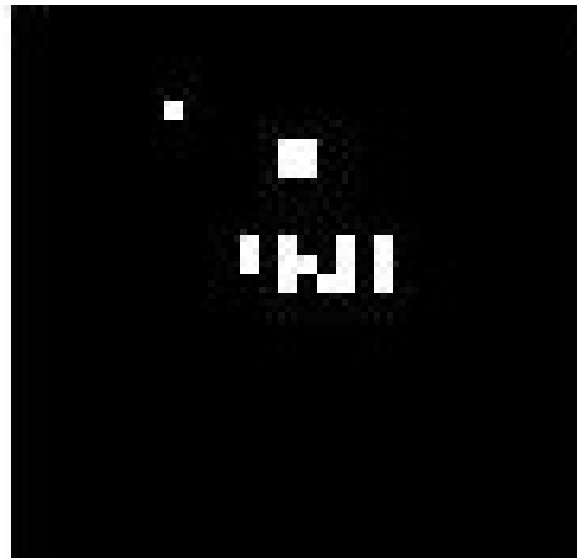


Figure 3.8 Output image by Pixel Swap

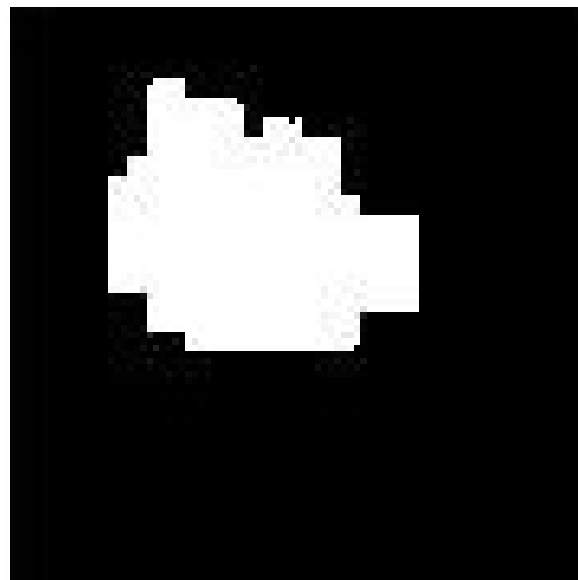


Figure 3.9 Output image by IED

However, the accuracy of both the output is checked by using the original Sentinel-2 10 m resolution imagery. The original Sentinel-2 imagery was also preprocessed. Preprocessing included endmember extraction by MEST, and preparation of abundance fraction map by LSU. The target pixels having an abundance fraction greater than 0.7 were used to quantify the accuracy of the outputs.

3.4.1 Mean Square Error (MSE)

It assesses the average of the squared difference between the original value and the predicted value [72]. The formula for the MSE is,

$$\sum \frac{(y_i - \hat{y}_i)^2}{n} \quad (3.4)$$

Here, y_i is the original value, \hat{y}_i is the predicted value and n is the number of observations.

All the values of the output pixel are subtracted from the pixel values of its corresponding pixel from the reference image, which is then taken average by the total number of pixels, i.e. 8100. The MSE obtained in the case of the PS algorithm was 80.5626, while for IDE, it was 1.1506.

3.4.2 Structural Similarity Index (SSI)

Image quality deterioration induced by processing such as data compression or data transmission losses is quantified using this perceptual metric [73]. This metric is based on the luminance, contrast, and structure of the image. SSI is the combination of luminance comparison function, contrast comparison function, and structure comparison function [74].

Using the built-in SSI function of MATLAB, SSI was calculated for both algorithms. For PS, the SSI came out to be 0.187, while for IED it came out to be 0.94.

3.4.3 Peak Signal to Noise Ratio (PSNR)

The peak signal-to-noise ratio (PSNR) is an expression for the ratio of a signal's greatest potential value (power) to the strength of distorting noise that influences its representation quality. The formula for PSNR involves MSE between the original image and the predicted image. Higher the PSNR value, the better the image quality.

Using a Python environment, the PSNR value of the original and predicted image is calculated. PSNR for the PS algorithm came out to be 18 dB, while for IED, it came out to be 51 dB.

3.4.4 Model Conclusion

Despite having low computational time than IED, various accuracy metrics pointed out that IED is better for the processing of Sentinel-2 imagery to perform subpixel mapping at a scale of 3. This method is further used in the next section to test on Landsat-8 30 m data.

CHAPTER 4

IMPLEMENTATION AND APPLICATIONS OF IED

4.1 DATA AND METHODOLOGY

4.1.1 Data Used

The data used for testing the model is from Landsat-8 satellite imagery. A 30×30 size image is downloaded with the help of Google Earth Engine. The spatial resolution of the image is 30 m. Figure 4.1 shows the image input.

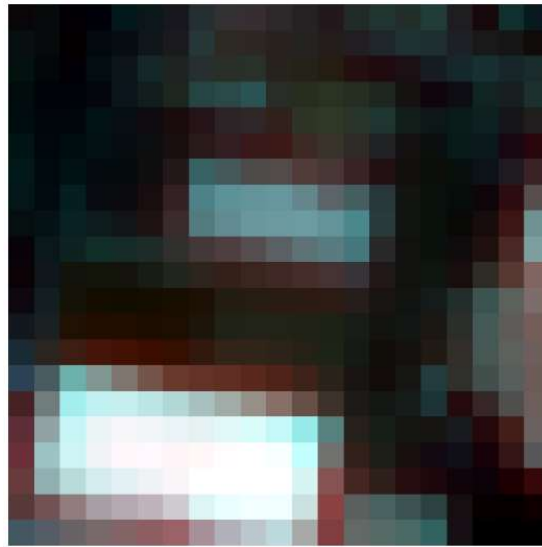


Figure 4.1 Landsat 30 m Imagery

4.1.2 Methodology

The testing aims to convert the 30 m spatial resolution Landsat data into 10 m spatial resolution by the process of the Inverse Euclidean Distance method of subpixel mapping. The process will be done, however, by considering two endmembers or classes only. The two classes are target and background. Target pixels are the pixels containing the roof (white colour in Figure 4.1) and the rest is the background. Figure 4.2 shows the flowchart of the methodology to be followed.

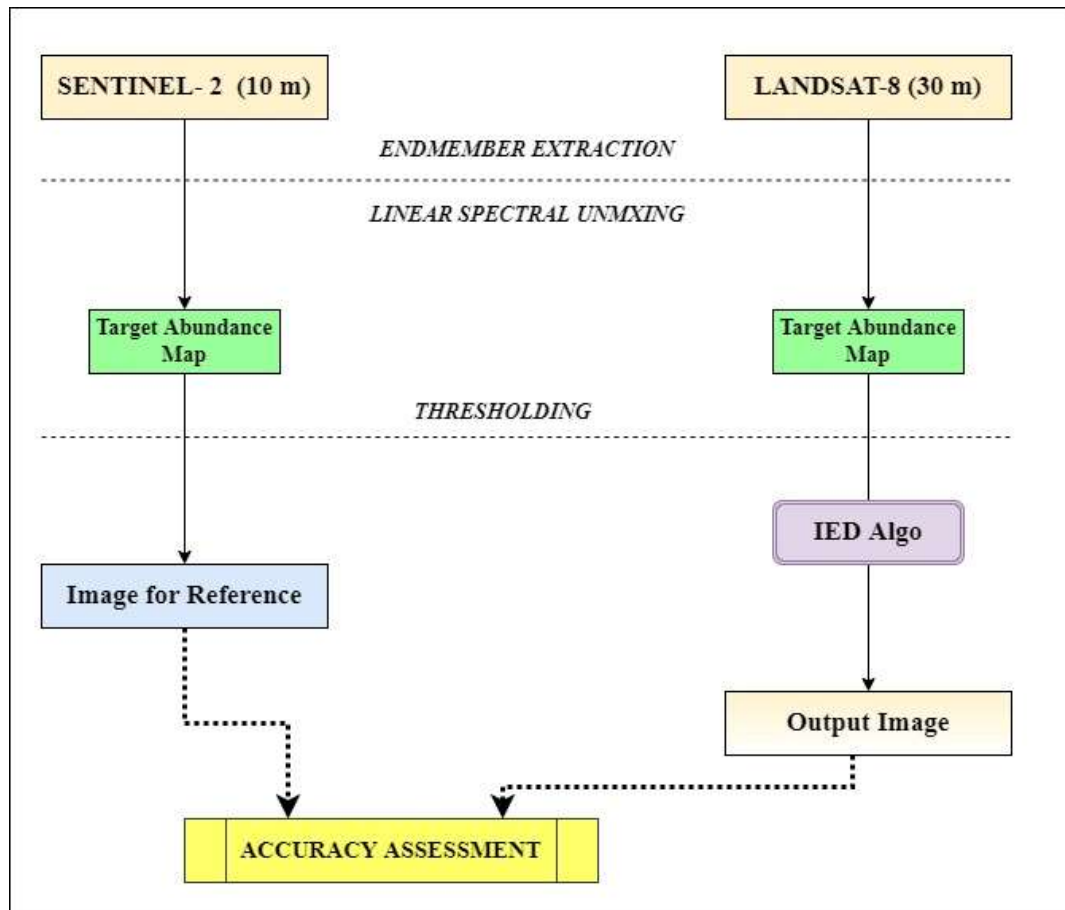


Figure 4.2 Flowchart of the methodology of testing

During the training phase of the model (Section 3.4), it was observed that the IED algorithm performs better than the PS algorithm. Therefore, it was selected for the testing phase. The observations of this phase are presented in the next section, and results and applications are presented in further sections.

4.2 IMPLEMENTATION

The data is first provided in ENVI Classic 5.3 for MEST and Linear Spectral Unmixing (LSU). The ROIs are created by human supervision, with constant attention to selecting pure pixels of the target as the required class (Figure 4.3). Figure 4.4 shows the abundance map of the target. This abundance map of the target is ingested into MATLAB R2019a. The histogram (Figure 4.5) of this abundance map is observed, for the threshold value of 0.78, as the target pixel. The image is then rescaled, in which the pixel with a cell value less than 0.78, is assigned 0 value, while the rest pixels are unchanged.



Figure 4.3 Endmember Selection using ROI tool in ENVI

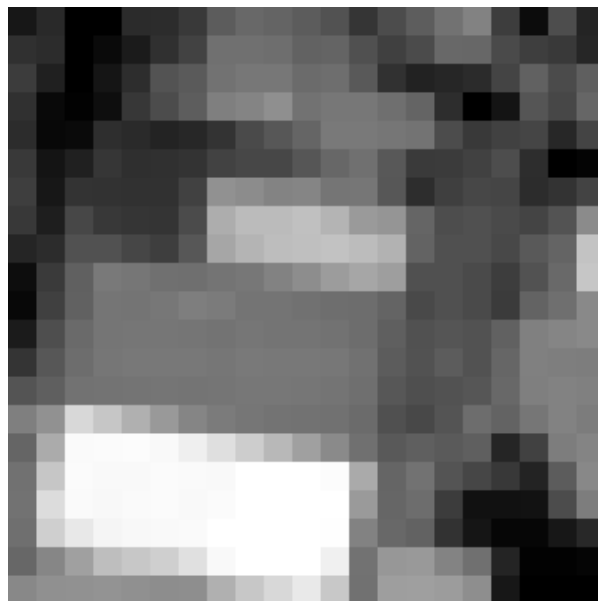


Figure 4.4 Abundance Map of Target

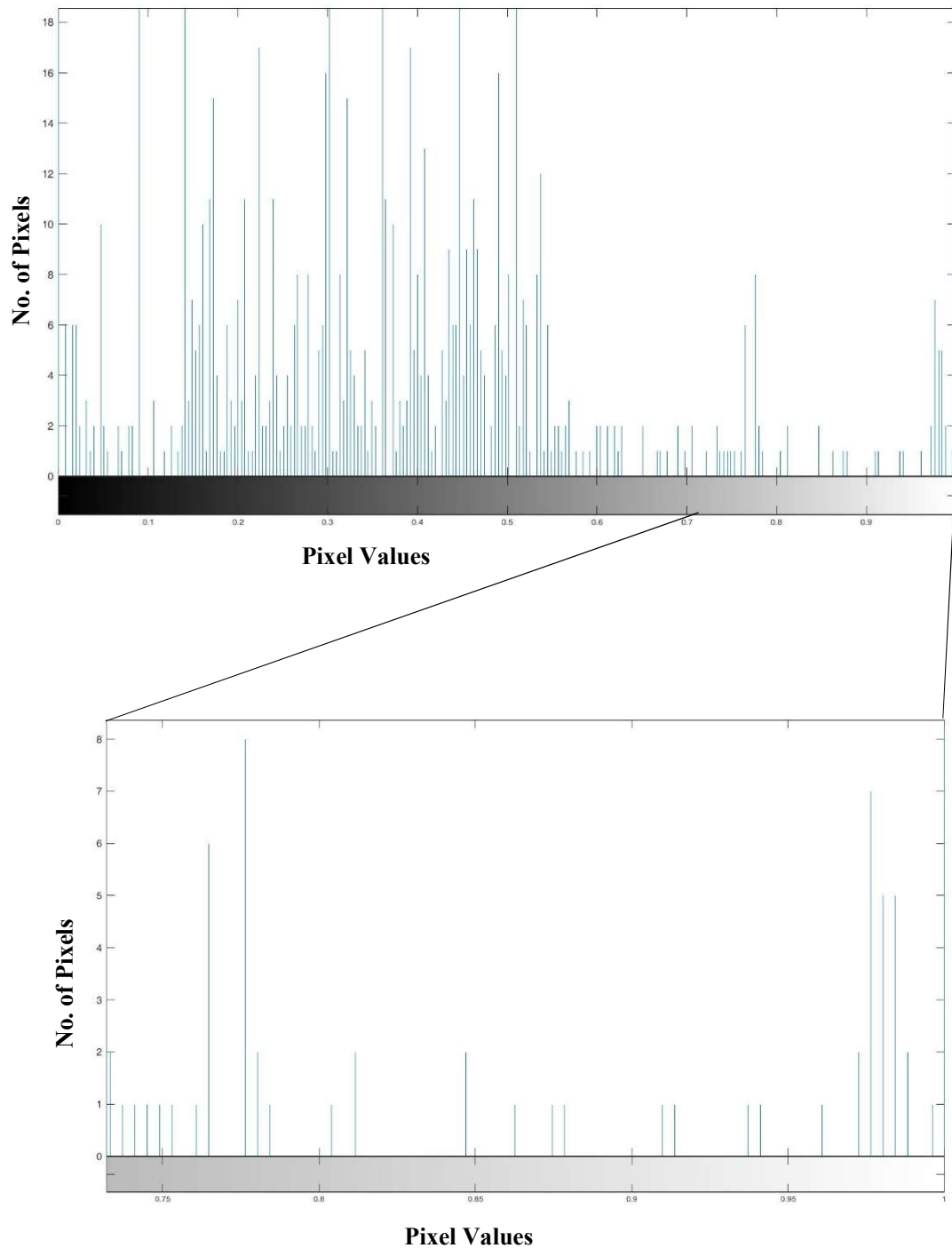


Figure 4.5 Histogram of the Landsat Data

Only a few pixels are having an abundance fraction greater than 0.78. Figure 4.6 shows the image after defining the threshold. This grayscale segmented image is then provided to the IED algorithm for subpixel mapping (Appendix 3). Figure 4.7 shows the output of the IED algorithm.

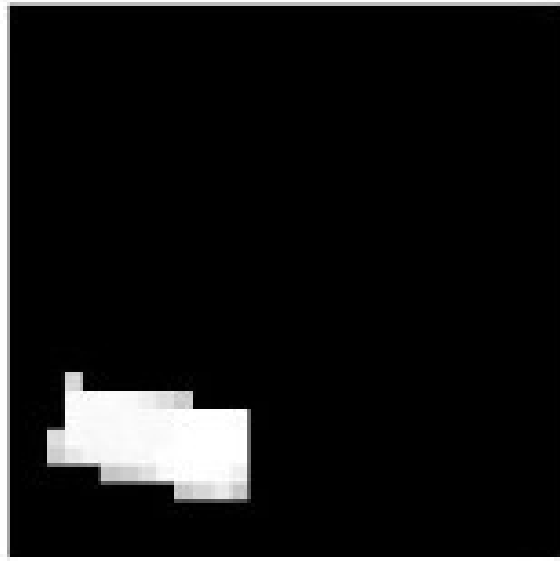


Figure 4.6 Target Image

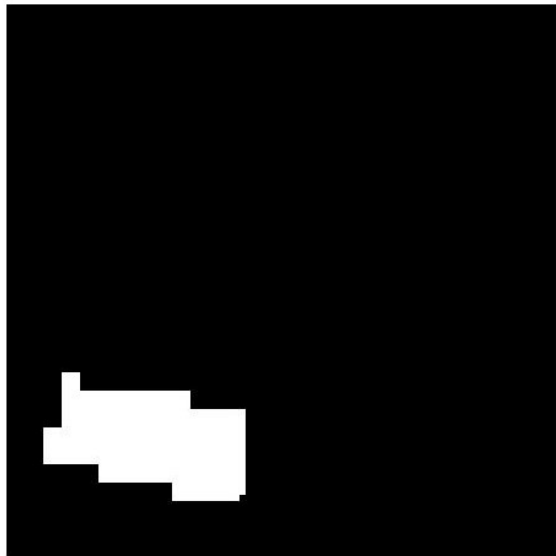


Figure 4.7 Output after IED Algorithm

The accuracy assessment of the output is done with the help of Sentinel-2 imagery of the same area and dimension. Figure 4.8 shows the RGB image of the Sentinel-2 data of the same region. Figure 4.9 shows its target abundance map. Thresholding the image for pixel value 0.78, and assigning 1 to the values above the threshold value, Figure 4.10 is obtained. This image is checked for accuracy with the output of the IED algorithm.

Sentinel-2 imagery is chosen for the process of validation, since, the spatial resolution of the Sentinel-2 is 10 m, and the spatial resolution of the data output is also 10 m.

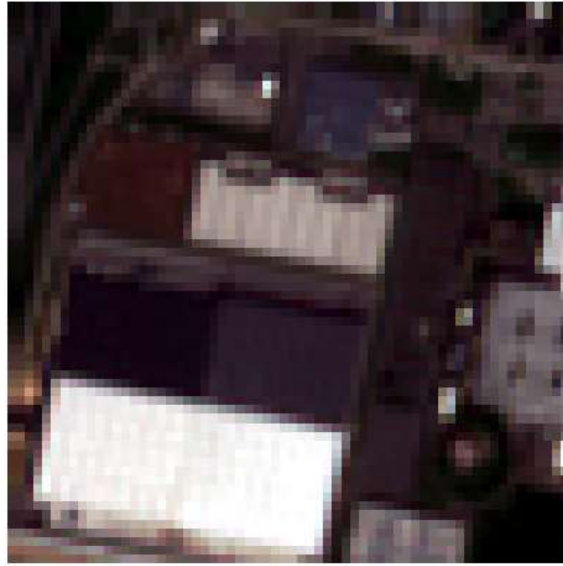


Figure 4.8 RGB Composite of Sentinel-2 data

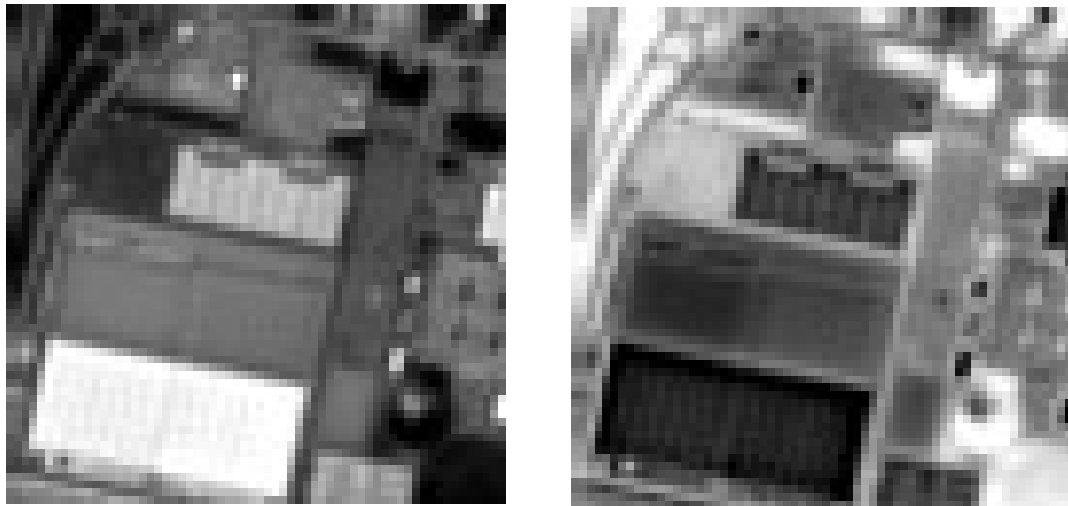


Figure 4.9 Abundance map of Target (left) and Background (right)



Figure 4.10 Binary Image of Sentinel-2 for validation

This binary image (Sentinel-2) is used for validation of the output from the IED algorithm.

4.3 AREA ESTIMATION

High-resolution satellite imagery has been used for the purpose of area estimation for a very long time [75] [76]. This study also has its application in the field of area estimation. Some assumptions for the process of area estimation change are:

- i. One pixel of a 10 m imagery is assigned an area of 1 square units.
- ii. One pixel of a 30 m imagery is assigned an area of 9 square units. This is because one pixel of a 30 m imagery is composed of 9 pixels of 10 m imagery.
- iii. Only full target pixels are considered for the calculation of area.
- iv. Targets are pixels having abundance fraction greater than 0.78.

For the process of area estimation, the area of all the pure target pixels is measured and compared for Sentinel-2 10 m imagery, Landsat-8 30 m imagery, and output image obtained by the IED subpixel mapping algorithm. The output image obtained has a spatial resolution of 10 m since the scale factor used in the study was 3.

4.4 RESULTS AND DISCUSSION

4.4.1 Results

The accuracy measures obtained are:

- i. The MSE error obtained is 5.196
- ii. The SSI obtained is 0.7358
- iii. The PSNR obtained is 32 dB

The area measures obtained from the three images in MATLAB are:

- i. The area of target in Sentinel-2 imagery is 504 square units.
- ii. The area of target in Landsat-8 imagery is 468 square units.
- iii. The area of target in IED output imagery is 486 square units

4.4.2 Discussion

The accuracy measures are not as high as obtained during the training phase. However, the measures are still reliable and can be improved by further changes in the method of endmember extraction and spectral unmixing. The loss in accuracy can be due to the selection of threshold value, or during the selection of endmember pure pixels. The increase in error is due to the misclassification of some target pixels into the background.

There has been a significant increase in the measurement of the area through this process of subpixel mapping. Area estimation by low-resolution satellite imagery is highly growing towards the actual calculated area (area through high resolution Sentinel-2 image).

CHAPTER 5

CONCLUSION

The high cost of fine-resolution satellite imagery has led to the inaccessibility of such data for civilian applications. Moreover, the inability to convert past low-resolution data to high resolution has led to the loss of temporal information. Super resolution of low-resolution imagery into high-resolution images is one of the most prominent solutions. The study is conducted to analyse the effect of two super resolution algorithms on the satellite imagery for binary target detection. Both of the algorithms are tested over Sentinel-2 original and resampled images. The image accuracy metrics, namely, Mean Squared Error (MSE), Peak Signal to Noise Ratio (PSNR), and Structural Similarity Index (SSI), concluded that the Inverse Euclidean Distance (IED) algorithm performs better as compared to Pixel Swapping Algorithm.

This algorithm is then used on Landsat-8 data, with a scale factor of 3, to obtain the high-resolution output image. This output image when compared with Sentinel-2 imagery of the same region, shows prominent accuracy. This output image, when tested for area estimation of the target region, showed a significant increase in the calculated value. The area, however, was still less than the actual area (area calculated by Sentinel-2 imagery).

The technique although producing good results has a limitation of working only on binary targets. The accuracy can be improved by choosing different types of endmember extraction and abundance mapping. Further study might employ non-linear abundance mapping methodologies and non-linear criteria for ranking subpixels for spatial distribution.

REFERENCES

- [1] X. Ma, Y. Hong, Y. Song and Y. Chen, "A Super-Resolution Convolutional-Neural-Network-Based Approach for Subpixel Mapping of Hyperspectral Images," *IEEE Journal Of Selected Topics In Applied Earth Observations And Remote Sensing*, 2019.
- [2] P. M. Atkinson, "Issues of uncertainty in super-resolution mapping and the design of an inter-comparison study," *Proc. 8th Int. Symp. Spatial Accur. Assessm. Natural Res. Envir. Sci.*, 2004.
- [3] A. Villa, J. Chanussot, J. A. Benediktsson, M. Ulfarsson and C. Jutten, "SUPER-RESOLUTION: An efficient method to improve spatial resolution of hyperspectral images," *IEEE International Geoscience and Remote Sensing Symposium*, 2010.
- [4] J. Chen, S. Yingying and L. Hengchao, "Processing and Analysis of Hyperspectral Data," 2020. [Online]. Available: <https://www.intechopen.com/books/processing-and-analysis-of-hyperspectral-data>.
- [5] M. Stuart, A. MvGonigle and J. Willmont, "Hyperspectral Imaging in Environmental Monitoring: A Review of Recent Developments and Technological Advances in Compact Field Deployable Systems.," *Sensors*, vol. 19, no. 14, p. 3071, 2019.
- [6] G. Vane, R. Green, T. Chrien, H. Enmark, E. Hansen and W. Porter, "The airborne visible/infrared imaging spectrometer (AVIRIS)," *Remote Sensing Environment*, 1993.
- [7] A. Cracknell, "Synergy in Remote Sensing: What's in a pixel?," *Int. J. Remote Sens.*, 1998.
- [8] X. Song, L. Zou and L. Wu, "Detection of Subpixel Targets on Hyperspectral Remote Sensing Imagery Based on Background Endmember Extraction," *IEEE Transactions on Geoscience and Remote Sensing*, 2020.
- [9] H. Xian-Hua, "Hyperspectral Image Super-resolution Using Optimization and DCNN-Based Methods, Processing and Analysis of Hyperspectral Data," 2019. [Online]. Available: <https://www.intechopen.com/chapters/69170>.
- [10] A. Marinoni, A. Plaza and P. Gamba, "A novel pre unmixing framework for efficient detection of linear mixtures in hyperspectral images," *IEEE Transactions on Geoscience and Remote Sensing*, vol. 55, no. 8, pp. 4325-4333, 2017.
- [11] M. Nachtgael, V. d. W. Dietrich, E. E. Kerre and W. Philips, *Soft Computing in Image Processing: Recent Advances*, 2007.
- [12] C. M. Lee, M. L. Cable, S. J. Hook, R. O. Green, S. L. Ustin, D. J. Mandl and E. M. Middleton, "An introduction to the NASA Hyperspectral InfraRed Imager (HypIRI) mission and preparatory activities," *Remote Sensing of Environment*, 2015.
- [13] J. Zhou, C. Kwan and B. Ayhan, "Improved target detection for hyperspectral images using hybrid in-scene calibration," *Journal of Applied Remote Sensing*, 2017.

- [14] J. Zhou, C. Kwan, B. Ayhan and M. T. Eismann, "A novel cluster kernel RX algorithm for anomaly and change detection using hyperspectral images," *IEEE Transactions on Geoscience and Remote Sensing*, 2016.
- [15] L. Yan, M. Zhao, X. Wang, Y. Zhang and J. Chen, "Object Detection in Hyperspectral Images," *IEEE Signal Processing Letters*, 2021.
- [16] R. A. McDonald, "Opening the Cold War sky to the public- Declassifying satellite reconnaissance imagery," *PE & RS- Photogrammetric Engineering and Remote Sensing*, vol. 61, no. 4, pp. 385-390, 1995.
- [17] T. Thierry and R. Chenier, "3-D radargrammetric modeling of RADARSAT-2 ultrafine mode: Preliminary results of the geometric calibration," *IEEE Geoscience and Remote Sensing Letters*, vol. 6, no. 2, pp. 282-286, 2009.
- [18] H. Topan, D. Maktav, K. Jacobsen and G. Buyuksalih, "Information content of optical satellite images for topographic mapping," *International Journal of Remote Sensing*, vol. 30, no. 7, pp. 1819-1827, 2009.
- [19] "Geocento Imagery," Geocento, [Online]. Available: <https://geocento.com/>. [Accessed 21 01 2022].
- [20] "Apollo Mapping: Image Hunters," Apollo Mapping, [Online]. Available: <https://apollomapping.com/>. [Accessed 21 01 2022].
- [21] "Satellite Data: What Spatial Resolution Is Enough?," Earth Observing System, [Online]. Available: <https://eos.com/blog/satellite-data-what-spatial-resolution-is-enough-for-you/>. [Accessed 01 21 2022].
- [22] A. Plaza, P. Martinez, R. Perez and J. Plaza, "A new approach to mixed pixel classification of hyperspectral imagery based on extended morphological profiles," *Pattern Recognition*, vol. 37, no. 6, pp. 1097-1116, 2004.
- [23] J. W. Boardman, F. A. Kruse and R. O. Green , "Mapping Target Signatures via partial unmixing of AVIRIS data," Pasadena, CA, 1995.
- [24] F. Kruse, A. Lefkoff , J. W. Boardman, K. Heiderbrecht, A. Shapiro , P. Barloon and A. Goetz, "The spectral image processing system (SIPS)—interactive visualization and analysis of imaging spectrometer data," *Remote Sens. Environ.*, vol. 44, pp. 145-163, 1993.
- [25] Q. Du and C.-I. Chang, "A linear constrained distance-based discriminant analysis for hyperspectral image classification," *Pattern Recognition*, vol. 34, no. 2, pp. 361-373, 2001.
- [26] H. G. Jones and X. R. R. Sirault, "Scaling of Thermal Images at Different Spatial Resolution: The Mixed Pixel Problem," *Agronomy*, vol. 3, no. 3, pp. 380-396, 2014.
- [27] L. Zhang, L. Zhang, D. Tao, X. Huang and B. Du, "Hyperspectral Remote Sensing Image Subpixel Target Detection Based on Supervised Metric Learning," *IEEE Transactions on Geoscience and Remote Sensing*, vol. 52, no. 8, pp. 4955-4965, 2014.
- [28] N. Keshava and J. F. Mustard, "Spectral Unmixing," *IEEE Signal Process. Mag.*, vol. 19, pp. 44-57, 2002.
- [29] R. S. Rand and D. M. Keenan, "A Spectral Mixture Process conditioned by Gibbs-based partitioning," *IEEE Trans. Geosci. Remote Sens.*, vol. 39, pp. 1421-1434, 2001.
- [30] C. C. Borel and S. A. W. Gerstl, "Nonlinear Spectral Mixing Models for Vegetative Soil Surfaces," *Remote Sens. Environ.*, vol. 47, pp. 403-416, 1994.

- [31] P. M. Mather, *Advances in Remote Sensing and GIS Analysis*, P. M. Atkinson and N. J. Tate, Eds., Chichester, West Sussex: Wiley, 1999.
- [32] C. I. Chang and Q. Du, "Estimation of Number of Spectrally Distinct Signal Sources in Hyperspectral Imagery," *IEEE Trans. Geosci. Remote Sens.*, vol. 42, no. 3, pp. 608-609, 2004.
- [33] K. V. Kale, M. M. Solankar and D. B. Nalawade, *Processing and Analysis of Hyperspectral Data*, J. Chen, Y. Song and H. Li, Eds., IntechOpen, 2019.
- [34] A. Zhang and Y. Xie, "Chaos Theory-Based Data-Mining Technique for Image Endmember Extraction: Laypunov Index and Correlation Dimension (L and D)," *IEEE Transactions On Geoscience And Remote Sensing*, vol. 52, no. 4, pp. 1935-1947, 2014.
- [35] P. J. Martinez, Perez R. M., A. Plaza, P. L. Aguilar, M. C. Cantero and J. Plaza, "Endmember extraction algorithms from hyperspectral images.," *Annals of Geophysics*, vol. 49, no. 1, 2006.
- [36] R. Song, J. P. Muller and A. Francis, "A Method of Retrieving 10-m Spectral Surface Albedo Products from Sentinel-2 and MODIS data," *IEEE International Geoscience and Remote Sensing Symposium IGARSS*, pp. 2381-2384, 2021.
- [37] A. Plaza, P. Martinez, R. Perez and J. Plaza, "A Quantitative and Comparative Analysis of Endmember Extraction Algorithms From Hyperspectral Data," *IEEE Transactions on Geoscience and Remote Sensing*, vol. 42, no. 3, pp. 650-663, 2004.
- [38] N. Keshava, "A Survey of Spectral Unmixing Algorithms," *Lincoln Lab*, vol. 14, no. 1, pp. 55-78, 2003.
- [39] S. Zhang, Y. Su, X. Xu, J. Li, C. Deng and A. Plaza, "Recent Advances in Hyperspectral Unmixing Using Sparse Techniques and Deep Learning," in *Hyperspectral Image Analysis. Advances in Computer Vision and Pattern Recognition*, S. Prasad and J. Chanussot, Eds., Springer, 2020.
- [40] J. Zhang, B. Rivard and A. Sanchez-Azofeifa, "Derivative Spectral Unmixing of Hyperspectral Data applied to mixtures of lichen and rock," *IEEE Trans. Geosci. Remote Sens.*, vol. 42, no. 9, pp. 1934-1940, 2004.
- [41] P. K. Garg, "Effect of Contamination and Adjacency Factors on Snow using Spectroradiometer and Hyperspectral Images," *Hyperspectral Remote Sensing*, pp. 167-196, 2020.
- [42] J. Yu, D. Chen, Y. Lin and S. Ye, "Comparison of Linear and Nonlinear Spectral Unmixing Approaches: A Case Study with Multispectral TM Imagery," *International Journal of Remote Sensing*, vol. 38, no. 3, pp. 773-795, 2017.
- [43] Y. Li, Y. Shi, K. Wang, B. Xi, J. Li and Gamba Paolo, "Target Detection with Unconstrained Linear Mixture Model and Hierarchical Denoising Autoencoder in Hyperspectral Imagery," *IEEE Transactions on Image Processing*, vol. 31, pp. 1418-1432, 2022.
- [44] T. Kasetkasem, M. K. Arora and P. K. Varshney, "Super Resolution Land Cover Mapping using a Markov Random field based approach," *Remote Sens. Environ.*, vol. 96, no. 3-4, pp. 302-314, 2005.
- [45] P. M. Atkinson, "Mapping Sub Pixel Boundaries from Remotely Sensed Images," *Innovations in GIS 4*, pp. 160-180, 1995.

- [46] F. Ling, Y. Du, F. Xiao, H. Xue and S. Wu, "Super-resolution land-cover mapping using multiple sub-pixel shifted remotely sensed images," *International Journal of Remote Sensing*, vol. 31, no. 19, pp. 5023-5040, 2010.
- [47] G. M. Foody, "Sharpening Fuzzy Classification Output to refine the Representation of Sub-pixel Land Cover Distribution," *International Journal of Remote Sensing*, vol. 19, pp. 2593-2599, 1998.
- [48] M. Q. Nguyen, P. M. Atkinson and H. G. Lewis, "Super resolution Mapping using a Hopfield Neural Network with Fused Images," *IEEE Transactions on Geoscience and Remote Sensing*, vol. 44, pp. 736-749, 2006.
- [49] P. Aplin and P. M. Atkinson, "Sub-pixel Land Cover Mapping for Per-field Classification," *International Journal of Remote Sensing*, vol. 22, pp. 2853-2858, 2001.
- [50] F. Ling, F. Xiao, Y. Du, H. Xue and X. Y. Ren, "Waterline Mapping at the Subpixel Scale from Remote Sensing Imagery with High-Resolution Digital Elevation Models," *International Journal of Remote Sensing*, vol. 29, pp. 1809-1812, 2008.
- [51] A. Deshpande and P. Patvardhan, "Survey of Super Resolution Techniques," *ICTACT Journal on Image & Video Processing*, vol. 9, no. 3, 2019.
- [52] J. Kim, K. Lee and K. M. Lee, "Accurate Image Super resolution using Very Deep Convolutional Networks," *IEEE Conference on Computer Vision and Pattern Recognition*, pp. 1646-1654, 2016.
- [53] H. Li, K. M. Lam and M. Wang, "Image Super resolution via Feature-augmented Random Forest," *Signal Processing: Image Communication*, vol. 72, pp. 25-34, 2019.
- [54] Z. Tang, M. Deng, C. Xiao and J. Yu, "Projection onto convex sets super-resolution image reconstruction based on wavelet bi-cubic interpolation," *Proceedings on 2011 International Conference on Electronic & Mechanical Engineering and Information Technology*, pp. 351-354, 2011.
- [55] K. C. Mertens, L. P. Verbeke, E. Ducheyne and R. R. De Wulf, "Using Genetic Algorithms in Sub-pixel Mapping," *International Journal of Remote Sensing*, vol. 24, no. 21, pp. 4241-4247, 2003.
- [56] K. C. Mertens, B. De Baets, L. P. Verbeke and R. R. De Wulf, "A Sub-pixel Mapping Algorithm based on Sub/pixel/pixel spatial attraction model," *International Journal of Remote Sensing*, vol. 15, no. 27, pp. 3293-3310, 2006.
- [57] K. Mertens, "Towards Sub-pixel Mapping: Design and Comparison of Techniques," Ghent University, 2008.
- [58] I. Izonin and A. Doroshenko, "Image Super-Resolution Techniques based on Machine Learning: Comparative Review," *Int. Rob. Auto J*, vol. 3, no. 7, 2017.
- [59] A. J. Tatem, G. L. Hugh, P. M. Atkinson and M. S. Nixon, "Super-Resolution Target Identification from Remotely Sensed Images Using a Hopfield Neural Network," *IEEE Transactions on Geoscience and Remote Sensing*, vol. 39, no. 4, p. 781, 2001.
- [60] J. P. Ardila, V. A. Tolpekin, W. Bijker and A. Stein, "Markov-Random-Field based Super-resolution Mapping for Identification of Urban Trees in VHR Images," *ISPRS Journal of Photogrammetry and Remote Sensing*, vol. 66, no. 6, pp. 762-775, 2011.

- [61] R. H. Kassaye, "Suitability of Markov Random Field based method for Super Resolution Land Cover Mapping," *ITC*, 2006.
- [62] J. Kennedy and R. Eberhart, "Particle Swarm Optimization," in *Proceedings of ICNN'95 - International Conference on Neural Networks*, 1995.
- [63] M. Li, W. Du and F. Nian, "An Adaptive Particle Swarm Optimization Algorithm Based on Directed Weighted Complex Network," *Mathematical Problems in Engineering*, vol. 2014, p. 7, 2014.
- [64] P. M. Atkinson, "Super-resolution Target Mapping from Soft-classified Remotely Sensed Imagery," in *Proceedings of the 5th International Conference on GeoComputation*, Leeds, UK, 2001.
- [65] P. M. Atkinson, "Sub-pixel Target Mapping from Soft-classified Remotely Sensed Imagery," *Photogrammetric Engineering & Remote Sensing*, vol. 71, no. 7, pp. 839-846, 2005.
- [66] M. K. Arora and K. C. Tiwari, "Subpixel Target Enhancement in Hyperspectral Images," *Defence Science Journal*, vol. 63, no. 1, pp. 63-68, 2013.
- [67] R. Fisher, S. Perkins, A. Walker and E. Wolfart, "Binary Images," 2003. [Online]. Available: <https://homepages.inf.ed.ac.uk/rbf/HIPR2/binimage.htm>.
- [68] J. Han, Y. Yu, K. Liang and H. Zhang, "Infrared Small-target Detection under Complex Background based on Subblock-level Ratio-difference Joint Local Contrast Measure," *Optical Engineering*, vol. 57, no. 10, 2018.
- [69] M. Kawulok, S. Piechaczek, K. Hrynchenko, P. Benecki, D. Kostrzewa and J. Nalepa, "On Training Deep Networks for Satellite Image Super-Resolution," *IGARSS 2019 IEEE International Geoscience and Remote Sensing Symposium*, pp. 3125-3128, 2019.
- [70] Y. F. Su, G. M. Foody, A. M. Muad and K. S. Cheng, "Combining Pixel Swapping and Contouring Methods to enhance Super-Resolution Mapping," *IEEE Journal of Selected Topics in Applied Earth Observations and Remote Sensing*, vol. 5, no. 5, pp. 1428-1437, 2012.
- [71] K. C. Tiwari, M. Arora and D. Singh, "Subpixel Target Detection and Enhancement in Hyperspectral Images," *Algorithms and Technologies for Multispectral, Hyperspectral and Ultraspectral Imagery XVII*, vol. 8048, 2011.
- [72] J. Frost, "Mean Squared Error (MSE)," Statistics By Jim, 2022. [Online]. Available: <https://statisticsbyjim.com/regression/mean-squared-error-mse/>.
- [73] "SSIM: Structural Similarity Index," imatest, [Online]. Available: <https://www.imatest.com/docs/ssim/#:~:text=Introduction%20%E2%80%94%20The%20Structural%20Similarity%20Index,by%20losses%20in%20data%20transmission..>
- [74] P. Datta, "All about Structural Similarity Index (SSIM): Theory + Code in PyTorch," Medium, Sept 2020. [Online]. Available: <https://medium.com/srm-mic/all-about-structural-similarity-index-ssim-theory-code-in-pytorch-6551b455541e>.
- [75] K. Grace, G. J. Husak, L. Harrison, D. Pederos and J. Michaelson, "Using High-resolution Satellite Imagery to Estimate Cropped Area in Guatemala and Haiti," *Applied Geography*, vol. 32, no. 2, pp. 433-440, 2012.
- [76] X. Liu and K. C. Clarke, "Estimation of Residential Population using High Resolution Satellite Imagery," in *Proceedings of the 3rd Symposium on Remote Sensing of Urban Area*, 2002.

- [77] R. B. Rustamov, H. Sabina and H. Z. Mahfuza, Multi-purposeful Application of Geospatial Data, BoD- Books on Demand, 2018.
- [78] M. M. Dalla, J. Benediktsson, J. Chanussot and L. Bruzzone, "The evolution of the morphological profile: from panchromatic to hyperspectral images," *Springer*, pp. 123-146, 2011.
- [80] A. Bateson and B. Curtiss, "A Method for Manual Endmember Selection and Spectral Unmixing," *Remote Sensing of Environment*, vol. 55, no. 3, pp. 229-243, 1996.
- [81] J. W. Boardman, F. A. Kruse and R. O. Green, "Mapping Target Signatures via Partial Unmixing of AVIRIS data," in *Summaries of the VI JPL Airborne Earth Science Workshop*, Pasadena, CA, 1995.
- [82] M. E. Winter, "N-FINDR: An Algorithm for Fast Autonomous Spectral Endmember Determination in Hyperspectral Data," *Proc. SPIE*, vol. 3753, pp. 266-275, 1999.
- [83] C. I. Chang and A. Plaza, "A Fast Iterative Algorithm for Implementation of Pixel Purity Index," *IEEE Geoscience and Remote Sensing Letters*, vol. 3, no. 1, pp. 63-67, 2006.
- [84] C. I. Chang, C. C. Wu and C. T. Tsai, "Random N-FINDR Endmember Extraction Algorithms for Hyperspectral Imagery," *IEEE Transactions on Image Processing*, vol. 20, no. 3, pp. 641-656, 2011.

APPENDIX 1

RESAMPLING CODE

```
import rasterio
from rasterio import Affine, Resampling
import os

path = '/content/drive/MyDrive/Data/Input/'
dest = '/content/drive/MyDrive/Data/Output/'

for filename in os.listdir(path):
    dat = os.path.join(path, filename)
    name = os.path.basename(dat)
    print(dat)
    print(name)

    def resample_raster(raster, scale=0.5):
        t = raster.transform

        #rescale the metadata
        transform = Affine(t.a / scale, t.b, t.c, t.d, t.e /
scale, t.f)
        height = raster.height * scale
        width = raster.width * scale

        profile = src.profile
        profile.update(transform=transform, driver='GTiff',
height=height, width=width, crs=src.crs)

        data = raster.read( #Note changed order of indexes,
arrays are band, row, col order not row, col, band
        out_shape=(int(raster.count), int(height),
int(width)),
        resampling=Resampling.bilinear)

        with rasterio.open(dest + name, 'w', **profile) as dst:
            dst.write(data)
            yield data

    with rasterio.open(dat) as src:
        with resample_raster(src, 1/3) as resampled:
            print('Orig dims: {}, New dims:
{}'.format(src.shape, resampled.shape))
            print(repr(resampled))
```

APPENDIX 2

PREPROCESSING OF DATA (MATLAB)

```
%Read image (abundance fraction of target)
img = imread('LSM_TAR.tif');

%Converting the uint8 type of image 2D matrix to double
type
img = double(img);

%Rescale the pixel values
bimg = img/255;

%View histogram to decide the threshold value
imhist(bimg);

%Thresholding the image to create binary image
bin = bimg>0.78;

%Viewing the binary image
imshow(bin)

%Saving the binary image as dat file
d = double(bin);
save input_image.dat -ascii
```

APPENDIX 3

IED TECHNIQUE (MATLAB)

```
% DISTANCE METHOD NEW FOR ANY PROPORTION BUT BINARY CASE

t1=cputime;
%lefttopcorner
load ('distlefttopcorner','distlefttopcorner');
    adist=distlefttopcorner;
clear distlefttopcorner

%Top middle centre
load ('disttopmiddlecentre','disttopmiddlecentre');
    bdist=disttopmiddlecentre;
clear disttopmiddlecentre

%Right top corner
load ('distrighttopcorner','distrighttopcorner');
    cdist=distrighttopcorner;
clear distrighttopcorner

%Left middle centre
load ('distleftmiddlecentre','distleftmiddlecentre');
    ddist=distleftmiddlecentre;
clear distleftmiddlecentre

%Right middle centre
load
('distrightmiddlecentre','distrightmiddlecentre');
    fdist=distrightmiddlecentre; % e LEFT TO MARK PIXEL
UNDER CONSIDERATION
clear distrightmiddlecentre

%Left Bottom corner
load ('distleftbottomcorner','distleftbottomcorner');
    gdist=distleftbottomcorner;
clear distleftbottomcorner

% bottom middle centre
load
('distbottommiddlecentre','distbottommiddlecentre');
    hdist=distbottommiddlecentre;
clear distbottommiddlecentre

%Right bottom corner
```

```

    load ('distrightbottomcorner', 'distrightbottomcorner');
    idist=distrightbottomcorner;
clear distrightbottomcorner

zoomfactor=3;
%+======
kzoom=zeros (zoomfactor*r, zoomfactor*c);
for m=1:1:r
    for n=1:1:c
        if k1(m,n)==1;
            kzoom(((m-1)*zoomfactor+1):zoomfactor*m), ((n-1)*zoomfactor+1):1:zoomfactor*n)=1;
        else
            if m==1
                if n==1
                    sumdist=zeros (zoomfactor, zoomfactor);

totclasspixels=round(k1(m,n)*zoomfactor*zoomfactor);

                    %Right middle centre
                    dist=fdist;

fraction=round((k1(m, (n+1))) *totclasspixels);
                    myplotdistance;
                    sumdisttemp=ksubback;
                    sumdist=sumdist+sumdisttemp;
                    clear sumdisttemp dist fraction
                    %figure, imshow(sumdist)

                    % Bottom middle centre
                    dist=hdist;

fraction=round((k1((m+1), (n))) *totclasspixels);
                    myplotdistance;
                    sumdisttemp=ksubback;
                    sumdist=sumdist+sumdisttemp;
                    clear sumdisttemp dist fraction
                    %figure, imshow(sumdist)

                    %Right bottom corner
                    dist=idist;

fraction=round((k1((m+1), (n+1))) *totclasspixels);
                    myplotdistance;
                    sumdisttemp=ksubback;
                    sumdist=sumdist+sumdisttemp;
                    clear sumdisttemp dist fraction
                    %figure, imshow(sumdist)

```

```

        kzoom(((m-
1)*zoomfactor+1):zoomfactor*m),((n-
1)*zoomfactor+1):1:zoomfactor*n))=sumdist;
        clear totalclasspixels sumdisttemp dist
fraction sumdist
        %figure,imshow(kzoom);

        elseif n==c
            sumdist=zeros(zoomfactor, zoomfactor);
totclasspixels=round(k1(m,n)*zoomfactor*zoomfactor);

            % Left middle centre
            dist=ddist;
            fraction=round((k1(m), (n-
1))) *totclasspixels);
            myplotdistance;
            sumdisttemp=ksubback;
            sumdist=sumdist+sumdisttemp;
            clear sumdisttemp dist fraction
            %figure,imshow(sumdist)

            % left bottom corner
            dist=gdist;
            fraction=round((k1(m+1), (n-
1))) *totclasspixels);
            myplotdistance;
            sumdisttemp=ksubback;
            sumdist=sumdist+sumdisttemp;
            clear sumdisttemp dist fraction
            %figure,imshow(sumdist)

            %Bottom middle centre
            dist=hdist;

fraction=round((k1(m+1), (n))) *totclasspixels);
            myplotdistance;
            sumdisttemp=ksubback;
            sumdist=sumdist+sumdisttemp;
            clear sumdisttemp dist fraction
            %figure,imshow(sumdist)

        kzoom(((m-
1)*zoomfactor+1):zoomfactor*m),((n-
1)*zoomfactor+1):1:zoomfactor*n))=sumdist;
        clear totalclasspixels sumdisttemp dist
fraction sumdist
        %figure,imshow(kzoom);

        else
            sumdist=zeros(zoomfactor, zoomfactor);
totclasspixels=round(k1(m,n)*zoomfactor*zoomfactor);

```

```

        % Left middle centre
        dist=ddist;
        fraction=round((k1((m),(n-
1))) *totclasspixels);
        myplotdistance;
        sumdisttemp=ksubback;
        sumdist=sumdist+sumdisttemp;
        clear sumdisttemp dist fraction
        %figure,imshow(sumdist)

        %Bottom middle centre
        dist=hdist;

fraction=round((k1((m+1),(n))) *totclasspixels);
        myplotdistance;
        sumdisttemp=ksubback;
        sumdist=sumdist+sumdisttemp;
        clear sumdisttemp dist fraction
        %figure,imshow(sumdist)

        %Right middle centre
        dist=fdist;

fraction=round((k1(m,(n+1))) *totclasspixels);
        myplotdistance;
        sumdisttemp=ksubback;
        sumdist=sumdist+sumdisttemp;
        clear sumdisttemp dist fraction
        %figure,imshow(sumdist)

        kzoom(((m-
1)*zoomfactor+1):zoomfactor*m),((n-
1)*zoomfactor+1):1:zoomfactor*n))=sumdist;
        clear totalclasspixels sumdisttemp dist
fraction sumdist
        %figure,imshow(kzoom);
        end
        %=====
        elseif m==r
            if n==1
                sumdist=zeros(zoomfactor, zoomfactor);

totclasspixels=round(k1(m,n) *zoomfactor*zoomfactor);

        %Right middle centre
        dist=fdist;

fraction=round((k1(m,(n+1))) *totclasspixels);
        myplotdistance;
        sumdisttemp=ksubback;

```

```

sumdist=sumdist+sumdisttemp;
clear sumdisttemp dist fraction
%figure,imshow(sumdist)

% Top middle centre
dist=bdist;
fraction=round((k1((m-
1),(n)))*totclasspixels);
myplotdistance;
sumdisttemp=ksubback;
sumdist=sumdist+sumdisttemp;
clear sumdisttemp dist fraction
%figure,imshow(sumdist)

%Right top corner
dist=cdist;
fraction=round((k1((m-
1),(n+1)))*totclasspixels);
myplotdistance;
sumdisttemp=ksubback;
sumdist=sumdist+sumdisttemp;
clear sumdisttemp dist fraction
%figure,imshow(sumdist)

kzoom(((m-
1)*zoomfactor+1):zoomfactor*m),((n-
1)*zoomfactor+1):1:zoomfactor*n)=sumdist;
clear totalclasspixels sumdisttemp dist
fraction sumdist
%figure,imshow(kzoom);
%=====
elseif n==c
sumdist=zeros(zoomfactor, zoomfactor);

totclasspixels=round(k1(m,n)*zoomfactor*zoomfactor);

%Left middle centre
dist=ddist;
fraction=round((k1((m),(n-
1)))*totclasspixels);
myplotdistance;
sumdisttemp=ksubback;
sumdist=sumdist+sumdisttemp;
clear sumdisttemp dist fraction
%figure,imshow(sumdist)

% Top middle centre
dist=bdist;
fraction=round((k1((m-
1),(n)))*totclasspixels);
myplotdistance;

```

```

sumdisttemp=ksubback;
sumdist=sumdist+sumdisttemp;
clear sumdisttemp dist fraction
%figure,imshow(sumdist)

%Left top corner
dist=adist;
fraction=round((k1((m-1),(n-
1))) *totclasspixels);
myplotdistance;
sumdisttemp=ksubback;
sumdist=sumdist+sumdisttemp;
clear sumdisttemp dist fraction
%figure,imshow(sumdist)

kzoom(((m-
1)*zoomfactor+1):zoomfactor*m),((n-
1)*zoomfactor+1):1:zoomfactor*n))=sumdist;
clear totalclasspixels sumdisttemp dist
fraction sumdist
%figure,imshow(kzoom);
else
sumdist=zeros(zoomfactor, zoomfactor);

totclasspixels=round(k1(m,n)*zoomfactor*zoomfactor);

%Left middle centre
dist=adist;
fraction=round((k1((m-1),(n-
1))) *totclasspixels);
myplotdistance;
sumdisttemp=ksubback;
sumdist=sumdist+sumdisttemp;
clear sumdisttemp dist fraction
%figure,imshow(sumdist)

% Top middle centre
dist=bdist;
fraction=round((k1((m-
1),(n))) *totclasspixels);
myplotdistance;
sumdisttemp=ksubback;
sumdist=sumdist+sumdisttemp;
clear sumdisttemp dist fraction
%figure,imshow(sumdist)

%Left top corner
dist=cdist;
fraction=round((k1((m-
1),(n+1))) *totclasspixels);
myplotdistance;

```



```

        sumdisttemp=ksubback;
        sumdist=sumdist+sumdisttemp;
        clear sumdisttemp dist fraction
        %figure,imshow(sumdist)

        kzoom(((m-
1)*zoomfactor+1):zoomfactor*m),((n-
1)*zoomfactor+1):1:zoomfactor*n))=sumdist;
        clear totalclasspixels sumdisttemp dist
fraction sumdist
        %figure,imshow(kzoom);
        end

    else
        if n==1
            %=====
            sumdist=zeros(zoomfactor, zoomfactor);

totclasspixels=round(k1(m,n)*zoomfactor*zoomfactor);

            % Top middle centre
            dist=bdist;
            fraction=round((k1((m-
1),(n)))*totclasspixels);
            myplotdistance;
            sumdisttemp=ksubback;
            sumdist=sumdist+sumdisttemp;
            clear sumdisttemp dist fraction
            %figure,imshow(sumdist)

            %Bottom middle centre
            dist=hdist;

fraction=round((k1((m+1),(n)))*totclasspixels);
            myplotdistance;
            sumdisttemp=ksubback;
            sumdist=sumdist+sumdisttemp;
            clear sumdisttemp dist fraction
            %figure,imshow(sumdist)

            %Right middle centre
            dist=fdist;

fraction=round((k1(m,(n+1)))*totclasspixels);
            myplotdistance;
            sumdisttemp=ksubback;
            sumdist=sumdist+sumdisttemp;
            clear sumdisttemp dist fraction
            %figure,imshow(sumdist)

```

```

        kzoom(((m-
1)*zoomfactor+1):zoomfactor*m),((n-
1)*zoomfactor+1):1:zoomfactor*n))=sumdist;
        clear totalclasspixels sumdisttemp dist
fraction sumdist
        %figure,imshow(kzoom);

        elseif n==c
        sumdist=zeros(zoomfactor, zoomfactor);

totclasspixels=round(k1(m,n)*zoomfactor*zoomfactor);

        % Top middle centre
        dist=bdist;
        fraction=round((k1((m-
1),(n)))*totclasspixels);
        myplotdistance;
        sumdisttemp=ksubback;
        sumdist=sumdist+sumdisttemp;
        clear sumdisttemp dist fraction
        %figure,imshow(sumdist)

        %Bottom middle centre
        dist=hdist;

fraction=round((k1((m+1),(n)))*totclasspixels);
        myplotdistance;
        sumdisttemp=ksubback;
        sumdist=sumdist+sumdisttemp;
        clear sumdisttemp dist fraction
        %figure,imshow(sumdist)

        %Left middle centre
        dist=ddist;
        fraction=round((k1((m),(n-
1)))*totclasspixels);
        myplotdistance;
        sumdisttemp=ksubback;
        sumdist=sumdist+sumdisttemp;
        clear sumdisttemp dist fraction
        %figure,imshow(sumdist)

        kzoom(((m-
1)*zoomfactor+1):zoomfactor*m),((n-
1)*zoomfactor+1):1:zoomfactor*n))=sumdist;
        clear totalclasspixels sumdisttemp dist
fraction sumdist
        %figure,imshow(kzoom);
        else
        %=====
        sumdist=zeros(zoomfactor, zoomfactor);

```

```

totclasspixels=round(k1(m,n)*zoomfactor*zoomfactor);

%Left top corner
dist=adist;
fraction=round((k1((m-
1),(n+1)))*totclasspixels);
myplotdistance;
sumdisttemp=ksubback;
sumdist=sumdist+sumdisttemp;
clear sumdisttemp dist fraction
%figure,imshow(sumdist)

% Top middle centre
dist=bdist;
fraction=round((k1((m-
1),(n)))*totclasspixels);
myplotdistance;
sumdisttemp=ksubback;
sumdist=sumdist+sumdisttemp;
clear sumdisttemp dist fraction
%figure,imshow(sumdist)

% Right Top corner
dist=cdist;
fraction=round((k1((m-
1),(n+1)))*totclasspixels);
myplotdistance;
sumdisttemp=ksubback;
sumdist=sumdist+sumdisttemp;
clear sumdisttemp dist fraction
%figure,imshow(sumdist)

%Left middle centre
dist=ddist;
fraction=round((k1((m),(n-
1)))*totclasspixels);
myplotdistance;
sumdisttemp=ksubback;
sumdist=sumdist+sumdisttemp;
clear sumdisttemp dist fraction
%figure,imshow(sumdist)

% Right middle Centre , The m, n is e which
is left
dist=fdist;

fraction=round((k1(m,(n+1)))*totclasspixels);
myplotdistance;
sumdisttemp=ksubback;
sumdist=sumdist+sumdisttemp;

```

```

clear sumdisttemp dist fraction
%figure,imshow(sumdist)

% left bottom corner
dist=gdist;
fraction=round((k1((m+1),(n-
1))) *totclasspixels);
myplotdistance;
sumdisttemp=ksubback;
sumdist=sumdist+sumdisttemp;
clear sumdisttemp dist fraction
%figure,imshow(sumdist)

%Bottom middle centre
dist=hdist;

fraction=round((k1((m+1),(n))) *totclasspixels);
myplotdistance;
sumdisttemp=ksubback;
sumdist=sumdist+sumdisttemp;
clear sumdisttemp dist fraction
%figure,imshow(sumdist)

%Right bottom corner
dist=idist;

fraction=round((k1((m+1),(n+1))) *totclasspixels);
myplotdistance;
sumdisttemp=ksubback;
sumdist=sumdist+sumdisttemp;
clear sumdisttemp dist fraction
%figure,imshow(sumdist)

kzoom(((m-
1)*zoomfactor+1):zoomfactor*m),((n-
1)*zoomfactor+1):1:zoomfactor*n)=sumdist;
clear totalclasspixels sumdisttemp dist
fraction sumdist
%figure,imshow(kzoom);
end
end
end
end
end
save output_tar.dat kzoom -ascii %image output save
figure,imshow(kzoom);
clear adist bdist cdist ddist edist fdist gdist hdist idist
t2=cputime;
Timetaken=t2-t1

```